78 Spectral Observables and Gauge Field Couplings in Causal Dynamical Triangulations

因果动态三角剖分中的 78 种谱可观测量与规范场耦合

Giuseppe Clemente and Massimo D’Elia

朱塞佩·克莱门特与马西莫·德利亚

Contents

目录

Abstract

摘要

In the first part of this Chapter, we discuss the role of spectral observables, describing possible ways to build them from discretizations of the Laplace-Beltrami operator on triangulations, and how to extract useful geometric information. In the second part, we discuss how to simulate the composite system of gauge fields coupled to CDT for generic groups and dimensions, showing results in some specific case and pointing out current challenges.

本章第一部分讨论谱可观测物理量的作用，阐述了从三角剖分上拉普拉斯-贝尔特拉米算子的离散化构造这类可观测物理量的可行方法，以及如何从中提取有用的几何信息。第二部分讨论如何模拟规范群耦合到因果动态三角剖分 (CDT) 的复合系统，适用于任意群与维度，并给出了若干特定情形的结果，同时指出当前面临的挑战。

G. Clemente (忠) M. D'Elia

G. 奇门蒂 (忠) M. 德利亚

Dipartimento di Fisica dell'Università di Pisa and INFN - Sezione di Pisa, Pisa, Italy e-mail: giuseppe.clemente@unipi.it; massimo.delia@unipi.it

意大利比萨大学物理系，意大利国家核物理研究所比萨分所，比萨，意大利邮箱:giuseppe.clemente@unipi.it；massimo.delia@unipi.it

---

Keywords

关键词

Quantum gravity - Causal dynamical triangulations - Spectral methods - Phase diagram - Lattice gauge theories - Gauge field topology

量子引力——因果动力学三角剖分——谱方法——相图——格点规范理论——规范场拓扑

Introduction

引言

One of the most promising results of pure-gravity CDT in 4D is that it appears to be non-perturbatively renormalizable in a Wilsonian renormalization group sense, i.e., there exist second-order critical points which are candidates for extracting continuous physics (see Chaps. 73, "Lattice Quantum Gravity: EDT and CDT" and - 82, "Semiclassical and Continuum Limits of Four-Dimensional CDT"). However, there is still an urge to identify a possibly complete set of physically meaningful observables to characterize all relevant features of the geometries under investigation.

四维纯引力 CDT 最具前景的结果之一是，它在威尔逊重整化群意义下似乎是非微扰可重整的，也就是说，存在可用于提取连续物理的二阶临界点 (参见第 73 章“格点量子引力:EDT 与 CDT”和第 82 章“四维 CDT 的半经典极限与连续极限”)。然而，我们仍需找到一套可能完整的、具有物理意义的可观测量，来表征所研究几何的所有相关特征。

The approach we followed in this respect is based on spectral methods, which are a set of techniques involving the analysis of eigenvalues and eigenvectors of dis-cretizations of the Laplace-Beltrami (LB) operators associated with spaces of functions on a manifold. One of the advantages of the spectral decomposition of the LB operators into eigenvalues and eigenvectors is contained in their hierarchical nature, which allows us to consistently separate large-scale features from short-scale ones; in general, the spectrum of a LB operator on a manifold M identifies a set of characteristic length scales, as we argue in section "Spectral Methods", while features like directionality, localization, and all the remaining metrical information can be extracted from eigenvectors, which take the role of waveforms (or diffusion) modes.

我们在这方面采用的方法基于谱方法，谱方法是一系列分析拉普拉斯-贝尔特拉米 (LB) 算子离散化的本征值与本征向量的技术，这类离散化对应流形上的函数空间。LB 算子按本征值与本征向量做谱分解的一大优势在于其分层性质，它让我们可以一致地分离大尺度特征与小尺度特征；正如我们在“谱方法”一节中论述的，一般而言，流形 M 上 LB 算子的谱确定了一组特征长度尺度，而方向性、局域化等特征以及其余所有度规信息都可以从本征向量中提取，本征向量在这里起到波形 (或扩散) 模式的作用。

Another direction that we investigated in order to extract meaningful physical properties of the system from CDT simulations is the problem of minimally coupling gravity and Yang-Mills gauge fields, possibly including also fermionic matter. Not only this is theoretically important in the search for a complete and self-consistently renormalizable quantum theory of gravity in the continuum, since the composite system could

possess different critical properties than the pure-gravity one but also because this allows an easier connection between the theory and possible phenomenological results from quantum cosmological observations, provided these would be available at some point. In section "Gauge Fields on Fluctuating Geometries", we describe the algorithmic strategies that we use to implement this minimal coupling and the challenges that appear for higher dimensions and gauge groups, both algorithmic and regarding the definition of meaningful observables.

为了从 CDT 模拟中提取系统有意义的物理性质，我们研究的另一个方向是引力与杨-米尔斯规范场(还可包含费米子物质) 的最小耦合问题。这一研究不仅在寻找连续空间中完整自洽可重整的量子引力理论层面具有理论重要性——因为复合系统可能拥有与纯引力系统不同的临界性质——而且还能让该理论更易于和未来可能获得的量子宇宙学观测唯象结果建立联系。在“涨落几何上的规范场”一节中，我们介绍了我们用来实现这种最小耦合的算法策略，以及高维和更大规范群面临的算法层面与可观测量定义层面的挑战。

Spectral Methods

谱方法

The relationship between the geometric properties of a manifold and the spectral decomposition of its associated Laplace-Beltrami (LB) operators is well known in literature [1-3], and spectral analysis, i.e., the study of eigenvalues and eigenvectors of relevant operators of the model under study, shows a wide spectrum of applications through science and beyond. In this section, we first introduce some basics regarding the physical role and interpretation of spectra and eigenvectors, followed by a graph discretization of the LB operator with some toy examples. Then, we show some numerical results for CDT and discuss other possible discretizations.

流形的几何性质与其关联拉普拉斯-贝尔特拉米 (LB) 算子谱分解的关系在文献中已被广泛熟知 [1-3]，而谱分析即对研究模型相关算子的特征值与特征向量的研究，在各科学领域及其他领域都有着广泛应用。本节我们首先介绍谱与特征向量的物理作用和诠释相关基础，随后通过几个简单示例给出 LB 算子的图离散化方案，最后展示 CDT 的部分数值结果，并讨论其他可行的离散化方法。

General Properties of Spectra and Eigenvectors

谱与特征向量的一般性质

In order to understand the physical content of the LB spectral decomposition, it is useful to start from the example of diffusion processes, for simplicity on boundaryless manifolds $\mathcal{M}$ (either smooth or piecewise flat, as the ones appearing in dynamical triangulations). On a chart with coordinates $\mathbf{x}$, and with diffusion time t (which is not a physical time), the heat equation takes the form:

为了理解 LB 谱分解的物理含义，我们可以从扩散过程的例子入手分析，为简化起见我们讨论无边界流形 $\mathcal{M}$ (包括光滑流形或分段平坦流形，例如动力三角化中出现的这类流形)。在带有坐标 $\mathbf{x}$ 的坐标卡中，扩散时间为 t (此处扩散时间并非物理时间)，热方程的形式为:

$$\partial_t u(\mathbf{x},t) = D^\mu D_\mu u(\mathbf{x},t), \tag{1}$$

where D_μ and $-D^\mu D_\mu$ are, respectively, the covariant derivative and the LB operator on $\mathcal{M}$. One then can proceed by expanding solutions on the basis of an orthonormal set of LB eigenfunctions $\phi_k(\mathbf{x})$ for each t

其中 D_μ 和 $-D^\mu D_\mu$ 分别是 $\mathcal{M}$ 上的协变导数与 LB 算子。我们可将方程解在 LB 特征函数的标准正交基 $\phi_k(\mathbf{x})$ 上展开，对任意 t 可得

$$u(\mathbf{x},t) = \sum_{k=0}^{\infty} c_k(t)\,\phi_k(\mathbf{x}), \tag{2}$$

and substitute into Eq. (1) to obtain

再将展开式代入式 (1) 得到

$$\frac{d}{dt}c_k(t) = -\lambda_k c_k(t) \;\rightarrow\; c_k(t) = c_k(0)\,e^{-\lambda_k t}, \tag{3}$$

with λ_k the eigenvalues of the LB operator associated to $\phi_k(\mathbf{x})$. The coefficients $c_n(0)$ are fixed by the initial condition $u(\mathbf{x},0)$. It is straightforward to show that the L_2 norm (weighted by the metric term $\sqrt{g(\mathbf{x})}$) of $u(\mathbf{x},t)$ is constant in diffusion time t, so we can interpret a solution with norm 1 as a probability distribution. In the case when one starts the diffusion process from a distribution where all probability is concentrated at one point $\mathbf{y}$, the fundamental solution to the heat equations

其中 λ_k 是 LB 算子对应于 $\phi_k(\mathbf{x})$ 的特征值。系数 $c_n(0)$ 由初始条件 $u(\mathbf{x},0)$ 确定。不难证明，$u(\mathbf{x},t)$ 的 L_2 范数 (由度量项 $\sqrt{g(\mathbf{x})}$ 加权) 在扩散时间 t 内保持不变，因此我们可以将范数为 1 的解解释为概率分布。如果扩散过程初始时所有概率都集中在单个点 $\mathbf{y}$，这个热方程的基本解

$$G(\mathbf{x},\mathbf{y};0) = \frac{1}{\sqrt{\det(g(\mathbf{x}))}}\delta^d(\mathbf{x}-\mathbf{y}), \tag{4}$$

$$\partial_t G(\mathbf{x},\mathbf{y};t) = D_x^2 G(\mathbf{x},\mathbf{y};t), \tag{5}$$

is the so-called heat-kernel, and it can be written either in terms of spectrum and eigenvectors of the LB operator or as an early (diffusion) time expansion, for any $\mathbf{x}$ and $\mathbf{y}$, reads as follows [4]:

就是所谓的热核，它可以通过 LB 算子的谱和特征向量表示，也可以写成扩散早期的展开形式，对任意 $\mathbf{x}$ 和 $\mathbf{y}$，表达式如下 [4]:

$$G(\mathbf{x},\mathbf{y};t) = \sum_{k=0}^{\infty} e^{-\lambda_k t}\phi_k(\mathbf{x})\,\phi_k(\mathbf{y}) \sim \left[\frac{e^{-d_g^2(\mathbf{x},\mathbf{y})/4t}}{(4\pi t)^{d/2}}\right]\sum_{n=0}^{\infty} a_n(\mathbf{x},\mathbf{y})\,t^n \tag{6}$$

where we denote by $d_g(\mathbf{x},\mathbf{y})$ the geodesic distance between the points $\mathbf{x}$ and $\mathbf{y}$. For a d -dimensional flat space, the term is square brackets of Eq. (6) is the only one present, because $a_0(\mathbf{x},\mathbf{y})$ is the only nonzero term in the series. Furthermore, for non-flat but smooth manifolds, the small t regime probes length scales of the order $d_g(\mathbf{x},\mathbf{y}) \sim \sqrt{t}$, due to the exponential falloff. This is connected to a property of the spectral version of the heat-kernel, appearing in the left expressions of Eq. (6), which consists in how eigenmodes

$\phi_k(\vec{x})$ with relatively larger eigenvalues λ_k are exponentially suppressed with respect to smaller eigenvalues. Indeed, this shows a key feature of the spectrum (even more evident if one considers the wave equation): the lowest part of the spectrum is associated to the slowest diffusion modes, while the highest part to the fastest. Since the eigenmodes of the LB operator are also solutions to the wave equation, a direct correspondence can be made between eigenvalues and the (inverse squares of the) wavelengths: in these terms, the lowest part of the spectrum is associated to the longest wavelengths (There is a disclaimer on the wave interpretation of eigenmodes: since the typical geometries we consider are random, the eigenmodes often exhibit an Anderson-like localization behavior [5, 6], instead of being long range.), while the highest eigenvalues are associated to the smallest ones, which, being related to the ultraviolet scales, can be neglected in the investigation of continuum physics. Another relevant quantity, related to the heat-kernel $G(\mathbf{x},\mathbf{y};t)$, is the average return probability [7-10], defined as

其中我们用 $d_g(\mathbf{x},\mathbf{y})$ 表示点 $\mathbf{x}$ 与 $\mathbf{y}$ 之间的测地线距离。对于 d 维平坦空间，式 (6) 方括号内就是唯一存在的项，因为 $a_0(\mathbf{x},\mathbf{y})$ 是级数中唯一的非零项。此外，对于非平坦的光滑流形，由于指数衰减，小 t 区域仅探测量级为 $d_g(\mathbf{x},\mathbf{y}) \sim \sqrt{t}$ 的长度尺度。这与式 (6) 左侧表达式中热核谱形式的性质有关: 特征模 $\phi_k(\vec{x})$ 中，特征值 λ_k 相对较大的模态相对于较小特征值的模态会被指数抑制。这确实体现了谱的一个关键特征 (如果考虑波动方程这一特征会更明显): 谱的低频部分对应最慢的扩散模式，高频部分对应最快的扩散模式。由于 LB 算子的特征模同时也是波动方程的解，因此可以在特征值与波长 (波长平方的倒数) 之间建立直接对应关系: 在此对应下，谱的低频部分对应最长波长 (对特征模的波动解释有一点需要说明: 由于我们研究的典型几何是随机的，特征模通常表现出类似安德森局域化的行为 [5, 6]，而非长程行为)，而最高特征值对应最短波长，最短波长与紫外尺度相关，因此在研究连续统物理时可以忽略。另一个与热核 $G(\mathbf{x},\mathbf{y};t)$ 相关的重要物理量是平均返回概率 [7-10]，定义为

$$P(t) := \frac{1}{\mathrm{Vol}(\mathcal{M})}\int d^d\mathbf{x}\sqrt{\det(g(\mathbf{x}))}G(\mathbf{x},\mathbf{x};t), \tag{7}$$

which can be analogously expanded in t as

它可以类似地在 t 中展开为

$$P(t) = \frac{1}{\mathrm{Vol}(\mathcal{M})}\sum_{k=0}^{\infty} e^{-\lambda_k t} \sim \frac{1}{(4\pi t)^{d/2}\,\mathrm{Vol}(\mathcal{M})}\sum_{n=0}^{\infty} A_n t^n. \tag{8}$$

The coefficients A_n are related to a useful hierarchy of geometric quantities such as volume ($A_0 = \mathrm{Vol}(\mathcal{M})$) , total curvature $\left(A_1 = \frac{1}{3}\int_{\mathcal{M}} R\right)$, and other diffeomorphism invariant scalars built from contractions of higher powers of the Riemann tensor [4, 11] . On a flat space $\mathbb{R}^d$, the return probability reduces to a power law behavior $P(t) = (4\pi t)^{-\frac{d}{2}}$ (with all coefficients $A_{i\geq 1} = 0$), as expected from scale invariance. For a (non-pathologically) curved but smooth manifold of dimension d , the leading diffusion behavior at small diffusion time acts is the same as the one of flat space with the same dimension. Therefore, in the case of a smooth manifold $\mathcal{M}$, just by using the LB spectrum, or equivalently by the return probabilities of diffusion processes at different diffusion times, it is possible to extract information about the dimension of the space:

系数 A_n 与体积 ($A_0 = \mathrm{Vol}(\mathcal{M})$)、总曲率 $\left(A_1 = \frac{1}{3}\int_{\mathcal{M}} R\right)$ 等有用的几何量分层结构，以及由黎曼张量更高次幂缩并构造的其他微分同胚不变标量 [4, 11] 相关。在平坦空间 $\mathbb{R}^d$ 中，返回概率呈现幂律行为 $P(t) = (4\pi t)^{-\frac{d}{2}}$ (所有系数为 $A_{i\geq 1} = 0$)，这符合标度不变性的预期。对于维度为 d 的 (非病态) 弯曲光滑流形，短扩散时间下的主导扩散行为和同维度平坦空间的扩散行为一致。因此，在光滑流形 $\mathcal{M}$ 的情况下，仅利用拉普拉斯-贝尔特拉米谱，或等价地通过扩散过程在不同扩散时间的返回概率，就可以提取空间维度的信息:

$$d = -2 \lim_{t\to 0^+} \frac{d\log P(t)}{d\log t}. \tag{9}$$

The geometries appearing in (C)DT are far from smooth, and that means that a small diffusion time extrapolation as the one shown in Eq. (9) is not really meaningful. However, one is not interested in the ultraviolet behavior, which is the one affected by discretization artifacts, but is sufficient to characterize geometries locally in a mesoscopic sense, i.e., for intermediate scales. Indeed, by universality arguments, the continuum limit behavior should be affected only by relevant operators which are insensitive to the finer details of the regularization. As we show in the next section, it is possible to extend the regime of validity of Eq. (9) up to finite diffusion times (instead of evaluating in the limit $t \to 0^+$) by defining the so-called spectral dimension, which can be evaluated at different diffusion times (or equivalently, length scales).

(因果) 动力学三角剖分中出现的几何远非光滑，这意味着式 (9) 所示的短扩散时间外推实际上没有意义。不过，我们并不关心受离散化 artifacts 影响的紫外行为，在介观尺度 (即中等尺度) 对几何做局部表征就足够了。实际上根据普遍性原理，连续极限行为仅受与正则化 finer details 无关的相关算符影响。正如我们在下一节展示的，通过定义可在不同扩散时间 (或等价地，不同长度尺度) 计算的所谓谱维数，可以将式 (9) 的有效范围拓展到有限扩散时间 (而非在 $t \to 0^+$ 极限下计算)。

Weyl's Law, Spectral Dimension, and Connectivity

外尔定律、谱维数与连通性

Let us consider again a d -dimensional smooth manifold $\mathcal{M}$ without boundaries and with spectrum $\sigma(\mathcal{M})$ of the LB operator. The count of eigenvalues below a spectral radius λ can be written as

我们再次考虑一个无边界的 d 维光滑流形 $\mathcal{M}$，其拉普拉斯-贝尔特拉米算子的谱为 $\sigma(\mathcal{M})$。小于谱半径 λ 的特征值个数可以写为

$$n(\lambda) \equiv \sum_{\lambda_k \in \sigma(\mathcal{M})} \theta(\lambda - \lambda_k) = \int_0^\lambda \rho(\lambda')\, d\lambda', \tag{10}$$

where we also defined the spectral density $\rho(\lambda) \equiv \frac{dn}{d\lambda} = \sum_k \delta(\lambda - \lambda_k)$. As clear from its definition in terms of eigenvalues, it is possible to write the return probability, shown in Eq. (8), as the Laplace transform of the spectral density $P(t) = \mathcal{L}[\rho(\lambda)](t)$. Likewise, the spectral density can then be written as an inverse Laplace transform of the return probability (This comes from the observation that the inverse Laplace transform of $\frac{1}{t^\alpha}$ is $\mathcal{L}^{-1}[t^{-\alpha}](\lambda) = \frac{\lambda^{\alpha-1}}{\Gamma(\alpha)}\theta(\lambda)$ and that $n(\lambda)$ is the integral of $\rho(\lambda)$.) $\rho(\lambda) = \mathcal{L}^{-1}[P(t)](\lambda)$ which, due to the leading small diffusion time behavior $P(t) \propto t^{-d/2}$, establishes a connection with another important

result of spectral geometry called Weyl's law [12, 13] , describing the asymptotic behavior of the eigenvalue counts $n(\lambda)$ at large spectral radius λ :

此处我们还定义了谱密度 $\rho(\lambda) \equiv \frac{dn}{d\lambda} = \sum_k \delta(\lambda - \lambda_k)$ 。从其基于特征值的定义可以看出，式 (8) 所示的返回概率可以写为谱密度 $P(t) = \mathcal{L}[\rho(\lambda)](t)$ 的拉普拉斯变换。同理，谱密度可写为返回概率的逆拉普拉斯变换 (这由以下观察推导而来: $\frac{1}{t^\alpha}$ 的逆拉普拉斯变换是 $\mathcal{L}^{-1}[t^{-\alpha}](\lambda) = \frac{\lambda^{\alpha-1}}{\Gamma(\alpha)}\theta(\lambda)$ ，且 $n(\lambda)$ 是 $\rho(\lambda)$ 的积分)。$\rho(\lambda) = \mathcal{L}^{-1}[P(t)](\lambda)$ ，结合扩散时间趋近于零时的主导行为 $P(t) \propto t^{-d/2}$ ，建立了它与谱几何中另一个重要结果外尔定律 [12, 13] 的联系，外尔定律描述了特征值计数 $n(\lambda)$ 在大谱半径 λ 下的渐近行为:

$$n(\lambda) \sim \frac{\omega_d V}{(2\pi)^d} \lambda^{d/2} \tag{11}$$

where ω_d is the volume of the d -dimensional ball of unit radius and $V \equiv \mathrm{Vol}(\mathcal{M})$ indicates the volume of the manifold. The leading dependence in expression in Eq. (11) can be used to build an alternative definition of the spectral dimension, which we call effective dimension [14], as a quantity that is in general running at different energy scales λ :

其中 ω_d 是单位半径 d 维球的体积，$V \equiv \mathrm{Vol}(\mathcal{M})$ 是流形的体积。利用式 (11) 中的主导依赖关系，可以给出谱维数的另一种定义，我们称之为有效维数 [14]，它是一个通常随能量标度 λ 变化的量:

$$d_{EFF}(\lambda) \equiv 2\frac{d\log(n/V)}{d\log\lambda}. \tag{12}$$

As mentioned in the previous section, another definition of dimension, called spectral dimension [8-10], can instead be defined in terms of return probability and diffusion times as an extension of the regime of validity of Eq. (9) to finite diffusion times t , namely,

如前一节所述，另一种维数定义即谱维数 [8-10]，可以通过返回概率和扩散时间定义，它是将式 (9) 的适用范围推广到有限扩散时间 t 得到的，即

$$D_S(t) \equiv -2\frac{d\log P}{d\log t}. \tag{13}$$

It should be evident at this point that the two definitions in Eqs. (12) and (13) are intimately connected through Laplace transform, which treats the diffusion time t and eigenvalue "energy" λ as variables dual to each other.

至此不难发现，式 (12) 和式 (13) 中的两种定义通过拉普拉斯变换紧密关联，拉普拉斯变换将扩散时间 t 和特征值“能量”λ 视为互为对偶的变量。

Before showing the results of the application in the CDT case, it is useful to see these definitions in action and get some intuition on their general behavior using some simplified toy examples on discretized geometries, for which the smoothness condition is not available, but where one can nevertheless extract geometric information at the mesoscopic scales.

在展示 CDT 情形下的应用结果之前，我们不妨先通过几个离散几何上的简化 toy 示例来看看这些定义的实际应用，建立对它们一般行为的直观认识；虽然这些离散几何不满足光滑性条件，但我们仍可以从中提取介观尺度的几何信息。

Let us consider a finite difference discretization of a three-dimensional torus as a regular cubic lattice, with, respectively, L_x, L_y , and L_z sites along three orthogonal directions. Eigenmodes are periodic plane waves $\phi_k\left(n_x, n_y, n_z\right) \propto\ e^{i(k_x n_x + k_y n_y + k_z n_z)}$ with wave number $\vec{k} = \left(k_x, k_y, k_z\right)$, where $k_i = 2\pi m_i / L_i$ and m_i integers such that $-L_i/2 < m_i \leq L_i/2$. Using $\vec{m}$, the spectrum can be written as

我们考虑三维环面的有限差分离散化，它是一个规则立方晶格，沿三个正交方向分别有 L_x, L_y 个和 L_z 个格点。本征模是周期平面波 $\phi_k\left(n_x, n_y, n_z\right) \propto\ e^{i(k_x n_x + k_y n_y + k_z n_z)}$ ，波数为 $\vec{k} = \left(k_x, k_y, k_z\right)$ ，其中 $k_i = 2\pi m_i / L_i$ 和 m_i 是满足 $-L_i/2 < m_i \leq L_i/2$ 的整数。利用 $\vec{m}$ ，谱可以写为

$$\lambda_{\vec{m}} = \sum_{\mu=x,y,z} 4\sin^2\left(\frac{\pi m_\mu}{L_\mu}\right), \tag{14}$$

but, for our applications, it is more useful to relabel them with a single integer label n and in nondecreasing order $\lambda_{n+1} \geq \lambda_n$. This allows us to use Eq. (12) to extract the effective dimension at different scales from the slope in log-log plots of λ_n versus the volume-normalized order $\frac{n}{V}$ (zero-mode excluded). Figure 1 shows, for different combinations of sizes L_i , how there is a quite well-defined scale separation between different eigenvalue ranges with different slopes and therefore different effective dimensions. In particular, notice in the right panel of Fig. 1 how the triangle and circle dots, associated with tori which differ only by L_z (and therefore the total volume), exhibit a collapse of their trends and the same slope behavior where transitions between different scaling dimensions happen at the same point in $\left(\lambda, \frac{n}{V}\right)$, which determines also the smallest eigenvalue or, equivalently, the largest linear size that can be reached. This shows that, using the volume-normalized order $\frac{n}{V}$ instead of just the eigenvalue order label n is essential to compare the spectra from triangulations with different volumes, as we do in section "Spectral Properties of CDT Configurations".

但对于我们的应用来说，用单个整数标记 n 并按非降序排列 $\lambda_{n+1} \geq \lambda_n$ 重新标记会更有用。这样我们就可以利用式 (12)，从 λ_n 对体积归一化阶数 $\frac{n}{V}$ (排除零模) 的双对数图中提取不同尺度的有效维数。图 1 展示了，对于不同的尺寸组合 L_i ，不同本征值区间存在相当清晰的尺度分离，它们对应不同的斜率，因此对应不同的有效维数。特别要注意的是，在图 1 的右图中，仅相差 L_z (因此总容积不同) 的两个环面对应的三角点和圆点，其趋势发生坍缩，且斜率行为相同——不同标度维数之间的转变在 $\left(\lambda, \frac{n}{V}\right)$ 的同一点发生，这一点同样决定了最小本征值，或者等价地说，决定了能达到的最大线性尺寸。这表明，就像我们在“CDT 构型的谱性质”一节中所做的那样，使用体积归一化阶数 $\frac{n}{V}$ 而非仅使用本征值阶数标记 n ，对于比较不同体积三角剖分的谱是至关重要的。

This example highlights also another important point: since the smallest nonzero eigenvalue, called spectral gap, sets the largest length scale of manifolds, it should vanish in the thermodynamical limit, i.e., when the volume diverges. In particular, we expect it to follow a power law behavior set by

这个例子还凸显了另一个要点: 被称为谱隙的最小非零本征值决定了流形的最大长度尺度，因此它在热力学极限 (即体积发散时) 应当趋于零。我们特别期望它遵循由下式确定的幂律行为

$$\lambda_1 \propto V^{-\frac{2}{d_{EFF,\,\mathrm{low}}}}, \tag{15}$$

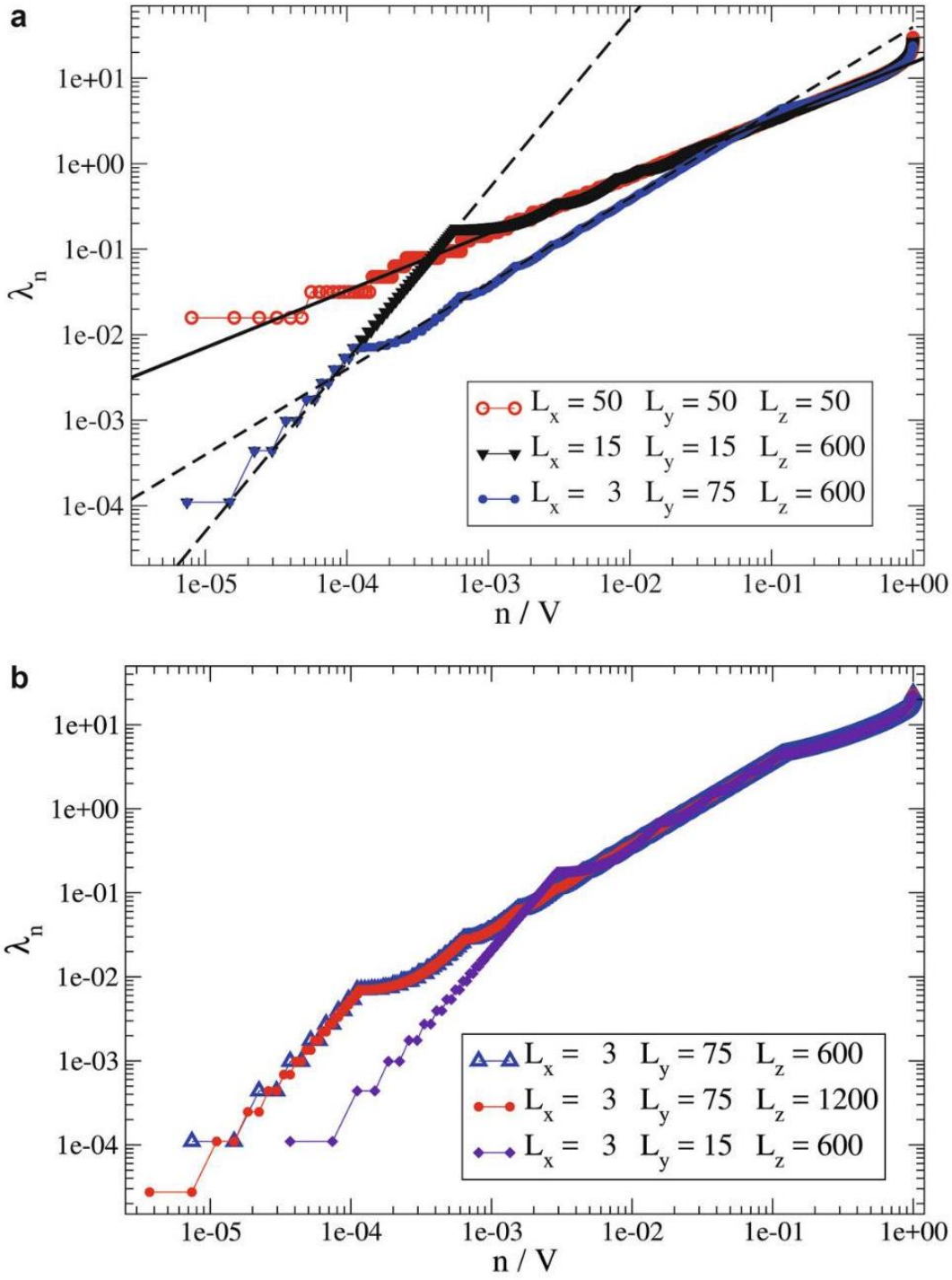

Fig. 1 Plots of λ_n against its volume-normalized order n/V , for a hypercubic lattice with periodic boundary conditions (i.e., toroidal) and different combinations of sizes L_i for each direction. The straight continuous line follows the exact Weyl scaling (see Eq. (11)) expected from a $d = 3$ dimensional space, while the dashed straight lines correspond to effective Weyl scalings for effective dimensions $d = 2$ and 1, which dominate the largest scale behavior

图 1 具有周期边界条件 (即环面) 的超立方晶格，在各方向尺寸取不同组合 L_i 时，λ_n 对其体积归一化阶数 n/V 的图。实线遵循 $d = 3$ 维空间预期的精确外尔标度 (见式 (11))，虚线则对应有效维数 $d = 2$ 和 1 的有效外尔标度，这两个维数主导大尺度行为

where $d_{EFF,\,\mathrm{low}}$ is the effective dimension in the lowest region of the spectrum (large scales). However, in section "Bifurcation Phase and $C_b - C_{dS}$ Phase Transition", we show that triangulations in the B phase and some slices in the bifurcation phase C_b possess a gap that does not vanish in the thermodynamical limit. This is related to the observation that geometries in those cases are typically highly connected and the effective dimension at larger scales is diverging, which is consistent with the relation in Eq. (15). The intimate relation between spectral gap and connectivity can be made more explicit. Indeed, a measure of connectivity for a compact Riemannian manifold $\mathcal{M}$ is encoded in the Cheeger isoperimetric constant $h(\mathcal{M})$, defined as the minimal area of a hypersurface ∂A which bipartitions $\mathcal{M}$ into two disjoint pieces A and $\mathcal{M} \setminus A$ in the most balanced way:

其中 $d_{EFF,\,\mathrm{low}}$ 是谱最低区域 (大尺度) 的有效维数。但在“分岔相和 $C_b - C_{dS}$ 相变”一节中，我们证明 B 相中的三角剖分以及分岔相 C_b 中的部分切片存在不随热力学极限消失的能隙。这与下述观测结果一致: 这些情况下的几何通常连通性很高，大尺度下的有效维数发散，这与式 (15) 的关系相符。谱隙和连通性之间的密切联系可以更明确地体现出来。事实上，紧致黎曼流形 $\mathcal{M}$ 连通性的度量蕴含在 Cheeger 等周常数 $h(\mathcal{M})$ 中，其定义为将 $\mathcal{M}$ 划分为两个不交部分 A 和 $\mathcal{M} \setminus A$ 的最均衡分划中，超曲面 ∂A 的最小面积:

$$h(\mathcal{M}) \equiv \inf \frac{\mathrm{Vol}\,(\partial A)}{\mathrm{Vol}\,(A)\,\mathrm{Vol}\,(\mathcal{M} \setminus A)}, \tag{16}$$

where the infimum is taken over all possible connected submanifolds A . The connectivity, in the form of the Cheeger constant, is bounded by the spectral gap through the: Cheeger inequality [15]

其中下确界是对所有可能的连通子流形 A 取的。连通性以切格常数的形式，通过切格不等式 [15] 被谱 gap 界定

$$h(\mathcal{M}) \leq 2\sqrt{\lambda_1} \tag{17}$$

Up to this point, we discussed general properties of spectra without referring to specific discretizations of the LB operator. In the next section, we introduce a graph discretization and show some results of the application of spectral analysis in CDT.

到目前为止，我们讨论了谱的一般性质，未涉及 LB 算子的具体离散化方法。在下一节中，我们将介绍图离散化，并展示谱分析在 CDT 中应用的一些结果

Graph Discretization of the Laplace-Beltrami Operator

拉普拉斯-贝尔特拉米算子的图离散化

Here, we discuss a specific class of discretizations of the Laplace-Beltrami operator on simplicial manifolds, namely, graph discretizations. In particular, we focus on the discretization as Laplace matrix on the

graph dual to the triangulation, where elementary blocks of space-time volumes, i.e., simplexes, are represented as nodes, while the adjacency relations between them are represented by links. In order to show how this discretization directly connects with functions on the continuous piecewise flat manifold, let us consider a scalar function $f(x)$ on a d -dimensional chart formed by a d -simplex σ_0 and all its adjacent simplexes $\{\sigma_k\}_{k=1,\ldots,d+1}$, assuming equilateral lengths of size a for each simplex (Fig. 2 illustrates the two-dimensional case).

我们在此讨论单纯流形上拉普拉斯-贝尔特拉米算子的一类特定离散化，即图离散化。我们特别关注与三角剖分对偶的图上的拉普拉斯矩阵离散化: 其中时空体积的基本单元 (即单纯形) 被表示为节点, 单纯形之间的邻接关系被表示为边。为说明该离散化如何直接关联连续分段平坦流形上的函数, 我们考虑标量函数 $f(x)$ 定义在由 d 维单纯形 σ_0 及其所有邻接单纯形 $\{\sigma_k\}_{k=1,\ldots,d+1}$ 构成的 d 维坐标图上，假设每个单纯形的边长均为等边长度 a (图 2 展示了二维情形)。

Since the space inside the chart is flat everywhere, one can Taylor expand around the barycenter $\vec{x}_0$ of σ_0 and with respect to the barycenters $\left\{\vec{x}_k = \vec{x}_0 + \delta\vec{x}_k\right\}_{k=1,\ldots,d+1}$ of the adjacent simplexes as follows:

由于坐标图内部空间处处平坦，我们可以围绕 σ_0 的重心 $\vec{x}_0$ ，对邻接单纯形的重心 $\left\{\vec{x}_k = \vec{x}_0 + \delta\vec{x}_k\right\}_{k=1,\ldots,d+1}$ 做如下泰勒展开:

$$f\left(\vec{x}_0 + \delta\vec{x}_k\right) = f\left(\vec{x}_0\right) + \delta x_k^i \partial_i f\left(\vec{x}_0\right) + \frac{1}{2}\delta x_k^i \partial_i \partial_j f\left(\vec{x}_0\right) \delta x_k^j + O\left(\left|\delta\vec{x}_k\right|^3\right). \tag{18}$$

In the equilateral case, the magnitude of the displacements $\delta\vec{x}_k$ is all proportional to the side lengths a , i.e., $\delta\vec{x}_k = \frac{a}{\sqrt{d+1}}\hat{v}_k$ for some unit vectors $\hat{v}_k$. Furthermore, the unit vectors all sum up to the zero vector $\sum_{k=1}^{d+1} \hat{v}_k = \vec{0}$, so one can eliminate the gradient term by summing over all displacements $\delta\vec{x}_k$. The best local approximation of the LB operator, using the function evaluation at the barycenters, is then given by (Summing over all displacements in the equilateral case results in $\sum_{k=1}^{d+1} \delta x_k^i \delta x_k^j = \frac{a^2}{d+1} \sum_{k=1}^{d+1} v_k^i v_k^j = a^2 \delta_{i,j}$.)

在等边情形下，位移 $\delta\vec{x}_k$ 的大小均与边长 a 成正比，即对单位向量 $\hat{v}_k$ 有 $\delta\vec{x}_k = \frac{a}{\sqrt{d+1}}\hat{v}_k$ 。此外，所有单位向量之和为零向量 $\sum_{k=1}^{d+1} \hat{v}_k = \vec{0}$ ，因此对所有位移 $\delta\vec{x}_k$ 求和即可消去梯度项。利用重心处的函数值，拉普拉斯-贝尔特拉米算子的最佳局部近似为 (对等边情形下所有位移求和可得 $\sum_{k=1}^{d+1} \delta x_k^i \delta x_k^j = \frac{a^2}{d+1} \sum_{k=1}^{d+1} v_k^i v_k^j = a^2 \delta_{i,j}$ 。)

$$-\Delta f\left(\vec{x}_0\right) = \frac{1}{a^2}\left[(d+1) f\left(\vec{x}_0\right) - \sum_{k=1}^{d+1} f\left(\vec{x}_k\right)\right] + O(a), \tag{19}$$

Fig. 2 Sketch of the dual graph discretization of the LB operator in 2D

图 2 二维下拉普拉斯-贝尔特拉米算子对偶图离散化示意图

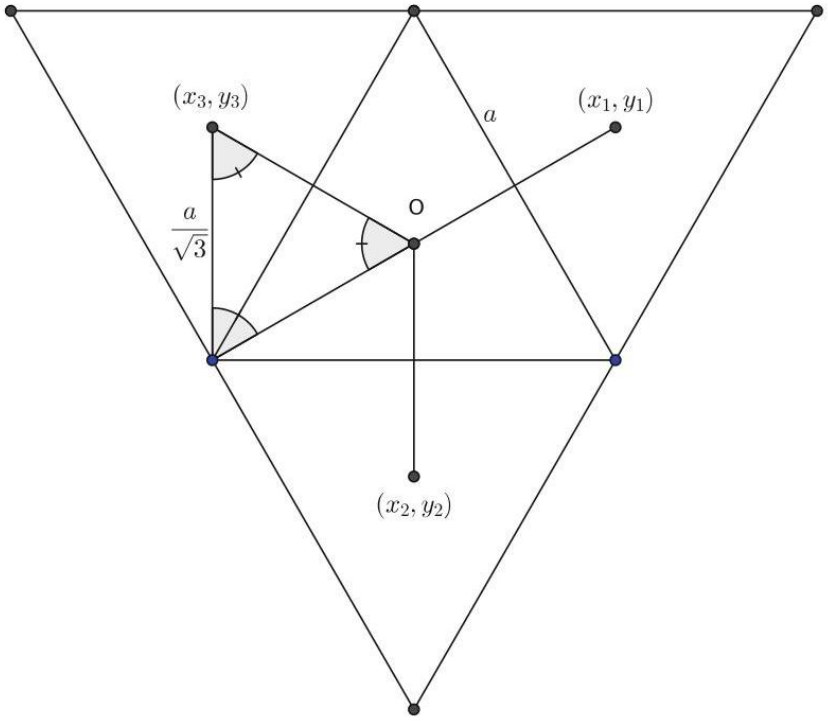

In this discretization, the space of scalar functions on the simplicial manifold can then be approximated by the set of values at the barycenter of each simplex $\{p_i\}_{i=0}^{|V|}$, i.e., $\vec{f} = \left(f(p_0), f(p_1), \dots, f\left(p_{|V|-1}\right)\right) \in \mathbb{K}$, for some field $\mathbb{K}$, while the LB operator takes the form of a matrix, called graph Laplacian:

在该离散化下，单纯流形上的标量函数空间可由每个单纯形 $\{p_i\}_{i=0}^{|V|}$ 重心处的函数值集合近似，即对某个场 $\mathbb{K}$ 有 $\vec{f} = \left(f(p_0), f(p_1), \dots, f\left(p_{|V|-1}\right)\right) \in \mathbb{K}$，同时拉普拉斯-贝尔特拉米算子呈现为矩阵形式，称为图拉普拉斯:

$$-\triangle \to L = (d+1) \cdot \mathbb{1} - A \tag{20}$$

where A is the adjacency matrix, whose entry A_{ij} is 1 if the simplexes labeled with i and j are adjacent and 0 otherwise.

其中 A 为邻接矩阵，若标记为 i 和 j 的单纯形相邻，则矩阵元素 A_{ij} 为 1，否则为 0。

In the next section, we show some results of the application of the dual graph Laplacian to investigate the geometric properties of CDT configurations.

下一节我们将展示应用对偶图拉普拉斯研究因果动态三角剖分构型几何性质的若干结果。

Spectral Properties of CDT Configurations

CDT 构型的谱性质

In previous sections, we introduced the main tools for spectral analysis. Here, we show some qualitative and quantitative results of their application. As discussed in Chaps. 73, "Lattice Quantum Gravity: EDT and CDT" and - 82, "Semiclassical and Continuum Limits of Four-Dimensional CDT", in four-dimensional CDT, there have been identified four phases, called A, B, C_{dS} , and C_b . These can be characterized in the first place by their typical volume profiles, i.e., the spatial volume per slice time $V_S(t)$. The A phase is considered unphysical since it exhibits small or absent correlation between adjacent slices, which is not observed in nature. B phase is also considered unphysical, since all space volume is concentrated on a slice. C_{dS} and C_b phases show instead spatial volumes more distributed in slice time and are therefore appealing for an investigation of the continuum limit, in particular at the transition between C_{dS} and C_b phases, which appears to be second order [16-19]. In the rest of this section and the next, we focus on the spectral properties of spatial slices of CDT configurations, since they capture the essential differences between phases, in particular for the C_b phase, discussed separately in section "Bifurcation Phase and $C_b - C_{dS}$ Phase Transition". As done in section "Weyl's Law, Spectral Dimension, and Connectivity", we can extract the effective dimension (12) from the slopes of $\lambda, n/V_S$ plots. Figure 3 shows the binned average of the collapsed curves in $\left(\lambda, \frac{n}{V_S}\right)$ for slices of some typical configurations, while Fig. 4 shows their corresponding effective dimension.

在前几节中，我们介绍了谱分析的主要工具。本节我们展示应用这些工具得到的若干定性与定量结果。正如第 73 章“格点量子引力:EDT 与 CDT”和第 82 章“四维 CDT 的半经典与连续极限”所讨论的，四维 CDT 中已识别出四个相，分别记为 A, B, C_{dS} 和 C_b 。它们首先可以通过典型体积剖面，即每一时间片 $V_S(t)$ 的空间体积来表征。A 相被认为是非物理的，因为它相邻切片之间的关联很小甚至不存在，这在自然界中无法观测到。B 相同样被认为是非物理的，因为所有空间体积都集中在单个切片上。而 C_{dS} 和 C_b 相的空间体积在时间上分布更均匀，因此适合研究连续极限，尤其是在 C_{dS} 和 C_b 相之间的转变处，该转变似乎是二阶相变 [16-19]。在本节剩余部分和下一节中，我们聚焦于 CDT 构型空间切片的谱性质，因为它们能够体现不同相之间的本质差异，尤其是将在“分岔相与 $C_b - C_{dS}$ 相变”一节单独讨论的 C_b 相。与“外尔定律、谱维数与连通性”一节的处理一致，我们可以从 $\lambda, n/V_S$ 图的斜率中提取有效维数 (12)。图 3 给出了 $\left(\lambda, \frac{n}{V_S}\right)$ 中典型构型切片坍缩曲线的分仓平均，图 4 则给出了对应的有效维数。

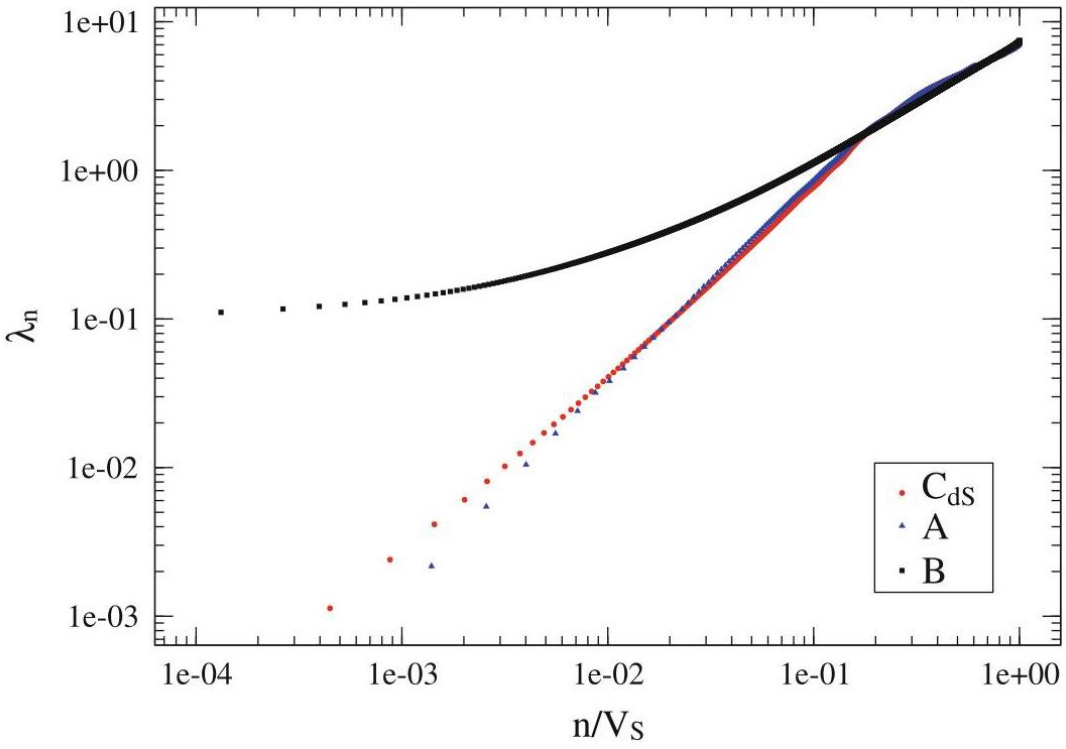

Fig. 3 Averages of λ_n versus n/V_S computed in bins of n/V_S with size $2/V_{S,\max}$ for slices taken from configurations sampled deep into the A, B , and C_{dS} phases. The volume is fixed to $V_{S,\,\mathrm{tot}} = 40k$ for configurations in A and C_{dS} phase and to $V_{S,\,\mathrm{tot}} = 8k$ for configurations in B phase. See Ref. [14] for details

图 3 取自深度采样自 A, B 相和 C_{dS} 相构型的切片，在 n/V_S 的尺寸为 $2/V_{S,\max}$ 的分仓中计算得到的 λ_n 对 n/V_S 的平均。对于 A 相和 C_{dS} 相的构型，体积固定为 $V_{S,\,\mathrm{tot}} = 40k$ ，对于 B 相的构型，体积固定为 $V_{S,\,\mathrm{tot}} = 8k$ 。详见文献 [14]

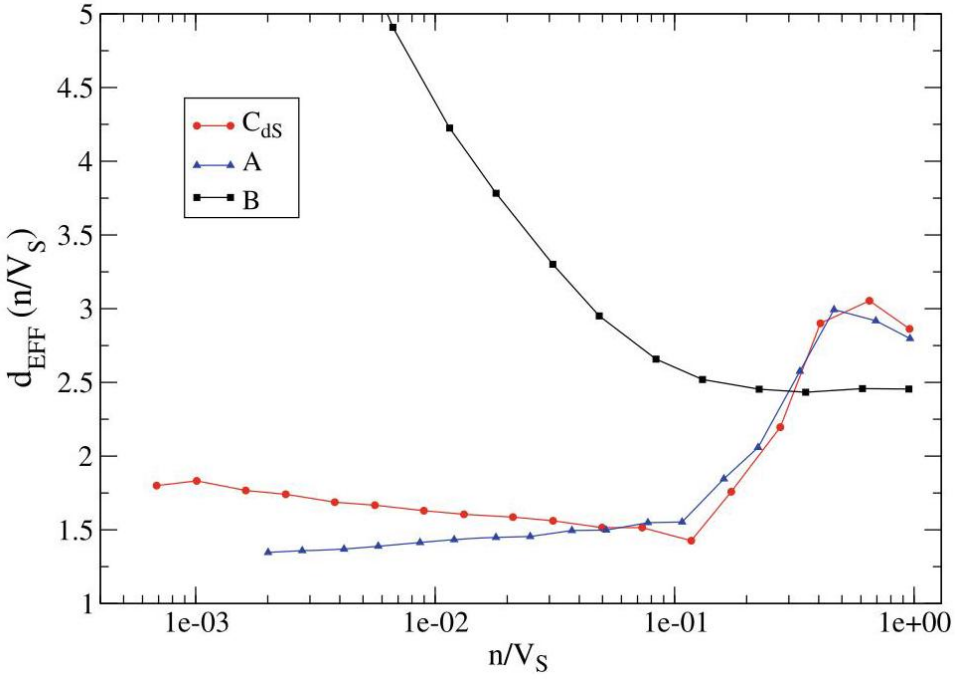

Fig. 4 Running dimension obtained from the logarithmic slope of λ vs $\frac{n}{V_S}$ curves (see section "Weyl's Law, Spectral Dimension, and Connectivity" and Eq. (12)), computed over windows of different ranges of n/V_S and for configurations sampled in phases C_{dS}, A , and B . The curve associated to the B phase is diverging for $n/V_S \to 0$ (it is around 30 at $n/V_S \sim 10^{-4}$), but part of it has been omitted from the plot, to improve the readability of the curves obtained for the other two phases. See Ref. [14] for details

图 4 由 λ 对 $\frac{n}{V_S}$ 曲线的对数斜率得到的跑动维数 (参见 "外尔定律、谱维数与连通性" 一节和式 (12)), 在 n/V_S 的不同范围窗口上对采样自 C_{dS}, A 相和 B 相的构型计算得到。对应 B 相的曲线在 $n/V_S \to 0$ 处发散 (在 $n/V_S \sim 10^{-4}$ 处约为 30), 但为了提升另外两个相曲线的可读性, 图中省略了该曲线的部分。详见文献 [14]

Notice how the single dominant slice in the B phase configurations has a diverging effective dimension on long range. As argued in section "Weyl's Law, Spectral Dimension, and Connectivity", this is related to a gapped spectrum with relatively large λ_1 , associated to a large connectivity of the geometry: since the spectral gap sets the largest scale possible, in B -phase slices, different regions are always quite close to each other, which accounts for the general geometry to be very connected. We are not interested in the properties of A -phase spatial slices, which appear to be vaguely similar to the one of C -phases slices, characterized by an almost constant effective dimension in a wide range of scales and with fractional value (the building blocks are three dimensional in this case). The behavior for $n/V_S \gtrsim 0.2 - 0.5$ should not be taken too seriously, since the corresponding values of λ are already close to the ultraviolet regime (see [14] for more details).

注意 B 位形中的单个主导片在长程上有效维度是发散的。正如在 "外尔定律、谱维度与连通性" 一节中论述的, 这与存在相对较大 λ_1 的有隙谱相关, 对应几何结构的高连通性: 由于谱隙设定了最大可能尺度, 在 B 相切片中, 不同区域之间始终相距很近, 这使得整体几何结构连通性很强。我们不关注 A 相空间切片的性质, 这类切片与 C 相切片大致相似, 其特点是在宽广尺度范围内有效维度几乎保持恒定且为分数值 (在该情况中结构基元是三维的)。不必太当真 $n/V_S \gtrsim 0.2 - 0.5$ 的行为, 因为对应的 λ 值已经接近紫外区域 (更多细节参见文献 [14])。

Bifurcation Phase and $C_b - C_{dS}$ Phase Transition

分岔相和 $C_b - C_{dS}$ 相变

Here, we complete the spectral characterization of slice geometries by considering the ensembles of configurations in the bifurcation phase C_b , which exhibits the same typical extended volume profile as the C_{dS} case, but which has been found to differ in the presence of a structure with vertex coordination numbers alternating in slice time between relatively small and large values. From this separation, C_b takes the name "bifurcation" phase. The methods are completely general, but in the following, we always discuss results for spatial slices with spherical topology. From the spectral point of view, Fig. 5 shows a qualitative comparison between the average spectral gaps (and a few higher-order eigenvalues) of C_{dS} and C_b slices as a function of the slice time. The alternating structure in slice time is quite noticeable in the slices from configurations in C_b phase, while it does not appear in the ones from C_{dS} phase. Furthermore, it is interesting to notice that for at some scale (around $\lambda \gtrsim \lambda_{100}$ in Fig. 5) how the qualitative dependence on the slice time seems to approach the C_{dS} one. Since relatively large spectral gaps are associated to highly connected geometries at large scales,

as we showed for B-phase slices, we can infer the geometry of C_b slices to be highly connected at larger scales.

本文我们通过研究分岔相 C_b 中的组态系综，完成切片几何的谱表征: 该相表现出与 C_{dS} 情形相同的典型扩展体积轮廓，但已发现其存在一种结构，顶点配位数沿切片时间在较小值与较大值之间交替。正是由于这种区分，C_b 被命名为“分岔”相。我们所用方法完全通用，但下文始终讨论球面拓扑空间切片的结果。从谱的角度看，图 5 定性比较了 C_{dS} 和 C_b 切片的平均谱隙 (以及几个高阶本征值) 随切片时间的变化。切片时间的交替结构在 C_b 相组态的切片中十分明显，在 C_{dS} 相的切片中则不存在。此外值得注意的是，在某一尺度下 (图 5 中约为 $\lambda \gtrsim \lambda_{100}$)，对切片时间的定性依赖似乎趋近于 C_{dS} 的情况。正如我们对 B 相切片的研究所示，较大的谱隙对应大尺度上高连通性的几何，因此我们可以推断，C_b 切片的几何在大尺度上是高连通的。

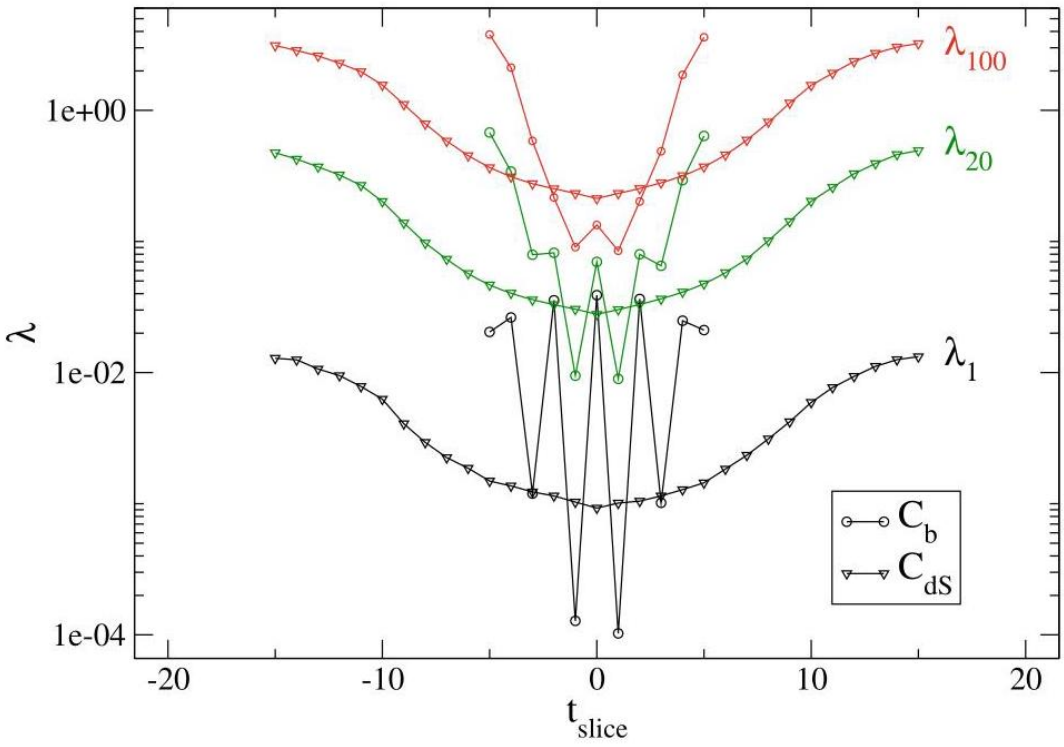

Fig. 5 Averages λ_1, λ_{20} , and λ_{100} for configurations in C_b and C_{dS} phases and as a function of the slice time. The slice time of maximal slices has been shifted to zero. See Ref. [14] for details

图 5 λ_1, λ_{20} 和 λ_{100} 是 C_b 相与 C_{dS} 相构型中对应物理量对切片时间的函数关系。极大切片的切片时间已平移至零。详见参考文献 [14]

As discussed in Chaps. 73, ”Lattice Quantum Gravity: EDT and CDT” and 82, ”Semiclassical and Continuum Limits of Four-Dimensional CDT”, it is apparent that C_{dS} and C_b are the only physically relevant phases. Indeed, the average spatial volume distribution observed for ensembles in the C_{dS} phase with spherical slice topology is in good agreement with what is expected from a de Sitter Universe, which corresponds to a S^4 geometry after analytical continuation to the Euclidean space [20]. Unlike C_{dS} , the bifurcation phase C_b is characterized instead by the presence of two different classes of slices that alternate each other in slice time t [18, 19] . This bifurcation behavior of C_b phase is apparent also from the general behavior of the aggregated spectrum of all slices as shown in Fig. 6 for three different values of $\Delta = 0.2, 0.4$, and 0.6, at the line with

constant $k_0 = 0.75$: inside the bifurcation phase, some slices are gapped, but increasing the value of Δ the gap disappears, and the two classes of slices merge into a common C_{dS} -like slice behavior. In particular, one can compute the average over an ensemble of configurations at fixed simulation parameters and the infinite volume extrapolation $\langle \lambda_n \rangle_\infty$ for each eigenvalue order n . On the left side vicinity of the critical point, this quantity follows a shifted power law:

正如第 73 章“格点量子引力:EDT 与 CDT”和第 82 章“四维 CDT 的半经典与连续极限”所讨论，显然 C_{dS} 和 C_b 是仅有的物理相关相。实际上，具有球面切片拓扑的 C_{dS} 相系综观测到的平均空间体积分布，与德西特宇宙的预期高度吻合，解析延拓到欧氏空间后对应 S^4 几何 [20]。与 C_{dS} 不同，分岔相 C_b 的特征是存在两类不同的切片，沿切片时间 t [18, 19] 交替出现。如图 6 所示，在恒定 $k_0 = 0.75$ 线上取三个不同 $\Delta = 0.2, 0.4$ 值 (其中一个为 0.6)，C_b 相的分岔行为也可从所有切片的聚合谱的整体行为中观察得到: 在分岔相内部，部分切片存在能隙，但随着 Δ 取值增大，能隙消失，两类切片合并为类似 C_{dS} 的共同切片行为。我们可以对固定模拟参数下的组态系综求平均，并对每一阶本征值 n 做无穷体积外推 $\langle \lambda_n \rangle_\infty$ 。在临界点左侧邻域，该量满足平移幂律:

$$\langle \lambda_n \rangle_\infty = A_n (\Delta - \Delta_c)^{2v}, \tag{21}$$

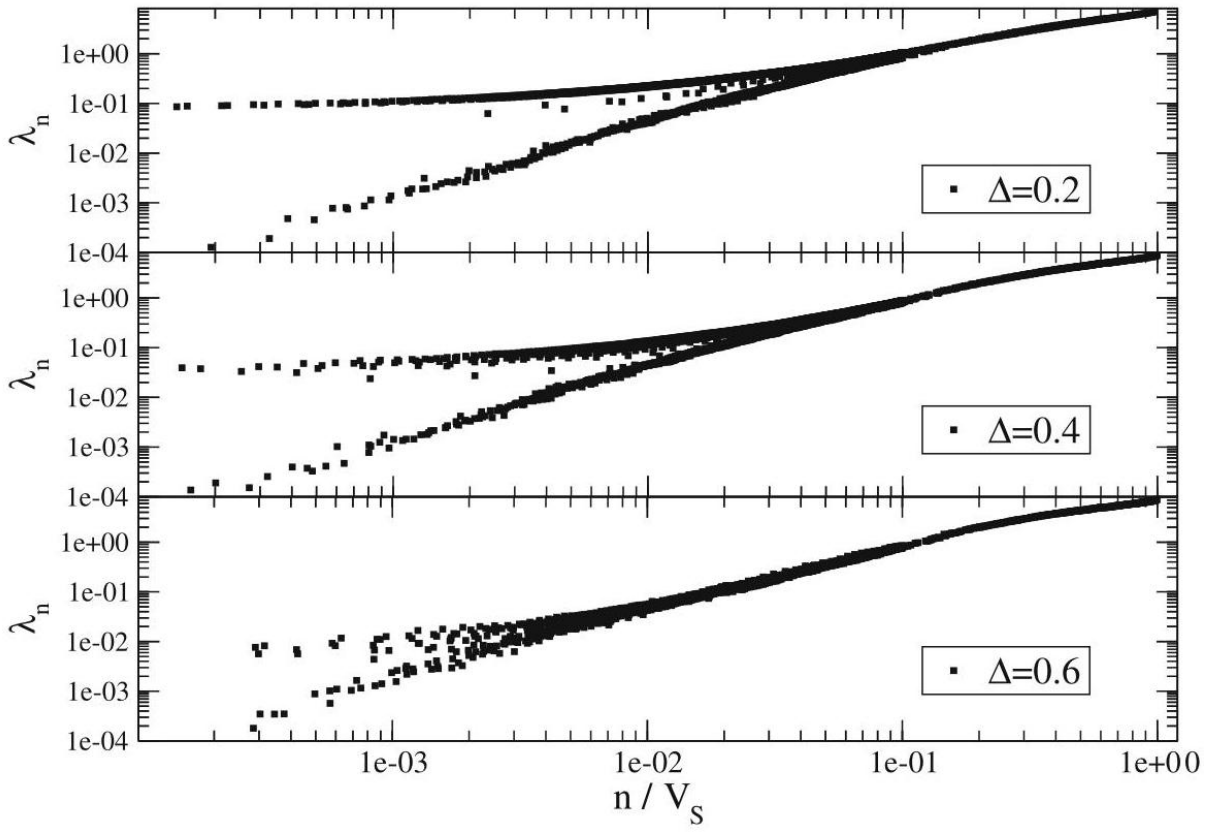

Fig. 6 Scatterplot of λ_n versus n/V_S for the slices (with spatial volume $V_S > 200$) of single configurations sampled at $k_0 = 0.75$ and for three different values of Δ in the C_b phase. See Ref. [14] for details

图 6 在 $k_0 = 0.75$ 处采样、处于 C_b 相的单个组态的所有切片 (空间体积为 $V_S > 200$) 中，λ_n 关于 n/V_S 的散点图，共对应三个不同的 Δ 取值，详见文献 [14]

where Δ_c and υ are in general functions of k_0 . Only the coefficients A_n of Eq. (21) depend on the eigenvalue order n , while υ appears to be the same for the lowest orders, with some tension for $n \gtrsim 10$.

其中 Δ_c 和 υ 通常为 k_0 的函数。仅式 (21) 的系数 A_n 依赖于本征值阶数 n ，对于最低阶，υ 始终保持一致，但对 $n \gtrsim 10$ 而言存在一定偏差。

For example, results of a combined fit with Eq. (21), including specifically the orders $n = 1$ and $n = 5$, are shown in Fig. 7 and yield $\Delta_c = 0.635\,(14), \upsilon = \ 0.55\,(4)$ for $k_0 = 0.75\left(\chi^2/\text{ d.o.f. } = 31/26\right)$ and $\Delta_c = 0.544\,(36), \upsilon = 0.82\,(12)$ for $k_0 = 1.50\left(\chi^2/\text{ d.o.f. } = 6/14\right)$ [29] .

例如，图 7 展示了结合式 (21) 对阶数 $n = 1$ 和 $n = 5$ 进行的联合拟合结果，拟合得到 $\Delta_c = 0.635\,(14), \upsilon = \ 0.55\,(4)$ 对应 $k_0 = 0.75\left(\chi^2/\text{ d.o.f. } = 31/26\right)$ ，$\Delta_c = 0.544\,(36), \upsilon = 0.82\,(12)$ 对应 $k_0 = 1.50\left(\chi^2/\text{ d.o.f. } = 6/14\right)$ [29] .

Since eigenvalues at each order n can be interpreted as distinct characteristic long-range lengths, the observation that they appear to scale with the same exponent υ suggests that a single length scale (e.g., the spectral gap λ_1) determines the general scaling behavior at the large length scales. This is reassuring because it is expected to happen when continuum physics behavior, where all quantities can be described by the scaling of a single characteristic length ξ , typically in the form of a correlation length. Therefore, gap between C_b and C_{dS} phases closes as expected from a second-order phase transition and for both the values of k_0 investigated.

由于每一阶 n 的本征值都可解读为不同的特征长程长度，本征值均服从同一标度指数 υ 的观测结果表明，单一长度尺度 (例如谱隙 λ_1) 决定了大尺度下的整体标度行为。这一结果符合预期，因为当系统呈现连续统物理行为时，所有物理量都可以通过单个特征长度 ξ 的标度行为描述，该特征长度通常为关联长度。因此，无论对所研究的任意 k_0 取值，C_b 相与 C_{dS} 相之间的能隙都符合二级相变的预期发生闭合。

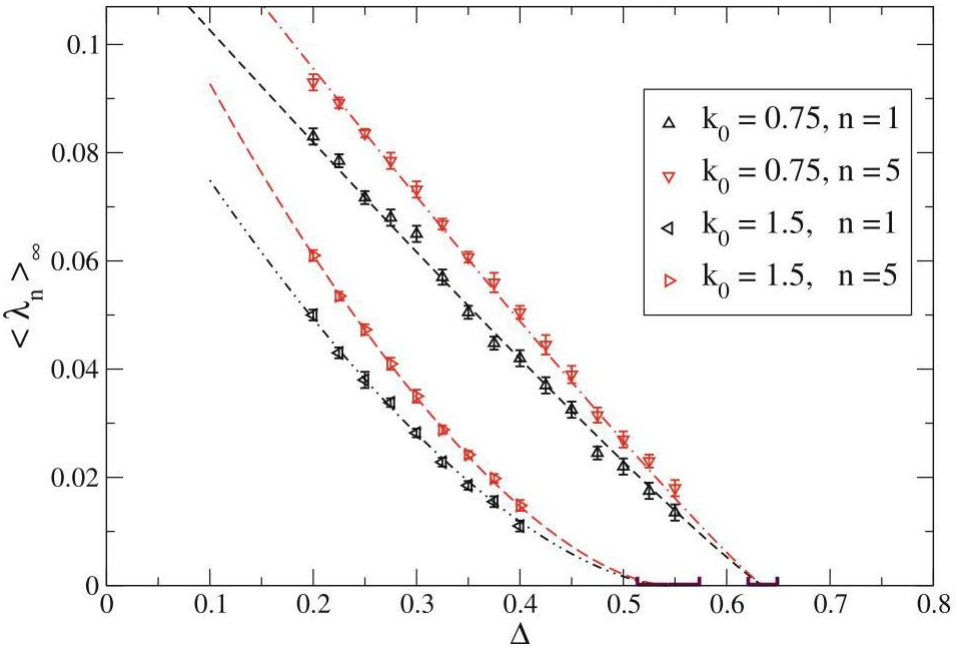

Fig. 7 Critical scaling of the spectral gap and lowest-order eigenvalues approaching the $C_b - C_{dS}$ phase transition and best fit with Eq. (21) [29]

图 7 趋近 $C_b - C_{dS}$ 相变时谱隙与最低阶本征值的临界标度，以及通过式 (21) 得到的最优拟合 [29]

An Alternative Approach to the Laplacian Discretization: Finite Element Methods

拉普拉斯离散化的替代方法: 有限元法

The graph discretization of the LB operator is certainly useful, but in general, other discretizations are possible, as well as extensions to the space of vector or tensor fields, as investigated in Ref. [21], where generalized spectral dimensions are defined. Here, we introduce a finite element discretization as an alternative tool that allows investigating some features not available in general with graph or other discretization in a consistent way. This section is based on Ref. [22], which should be referred to for a more detailed discussion.

拉普拉斯-贝尔特拉米 (LB) 算子的图离散化固然有用，但一般而言还存在其他离散化方式，也可拓展至向量场或张量场空间，正如文献 [21] 所研究的，其中定义了广义谱维数。在此我们引入有限元离散化作为替代工具，它能够以一致的方式研究图离散化或其他一般离散化方法通常无法实现的部分特性。本节基于文献 [22] 撰写，更深入的讨论可参阅该文献。

Weak Formulation and the Finite Element Methods

弱公式化与有限元方法

The name finite element methods (FEM) covers a wide family of approximation techniques that are applied in many fields, where complex modeling is necessary, to numerically solve very general integrodifferential equations [23-27]. As we describe in more detail in the following, the general procedure consists in casting the components of the problem under investigation into simpler and smaller parts, which makes the problem easier to be treated numerically.

有限元方法 (FEM) 涵盖了范围广泛的近似技术，应用于许多需要复杂建模的领域，用于对非常一般的积分微分方程进行数值求解 [23-27]。正如我们下文将更详细介绍的，该方法的一般流程是将待研究问题拆分为更简单的更小部分，从而让问题更便于数值处理。

In the context of performing spectral analysis of general manifolds, FEM consists in casting the LB eigenproblem

在对一般流形做谱分析的场景下，有限元方法将拉普拉斯-贝尔特拉米特征值问题

$$-\triangle f(\mathbf{x}) = \lambda f(\mathbf{x}). \tag{22}$$

into a weak formulation by multiplying both sides by a test function $\phi(\vec{x})$ and integrating everywhere, which results, for a boundaryless manifold $\mathcal{M}$, in

转化为弱公式化: 将方程两边乘以测试函数 $\phi(\vec{x})$ 后在全域积分，对于无边界流形 $\mathcal{M}$ ，可得

$$\int_{\mathcal{M}} d^d x \nabla\phi(\mathbf{x}) \nabla f(\mathbf{x}) = \lambda \int_{\mathcal{M}} d^d x \phi(\mathbf{x}) f(\mathbf{x}), \tag{23}$$

where integration by parts has been performed on the left side. The test function ϕ can belong to different classes of functions, but it is customary for the LB eigenproblem to consider the Sobolev space $H^1(\mathcal{M})$, or simply H^1 , defined as the space of L^2 functions that admit weak first derivatives, since the problem is well posed and solutions are proven to exist. We want to stress that, for a piecewise linear manifold $\mathcal{M}$, the Sobolev space $H^1(\mathcal{M})$ involves all functions on the whole domain of the manifold, i.e., not just the vertices or the simplexes centers but also the interior of flat simplexes. In the following, we call the spectrum of the Laplace-Beltrami operator on the space of functions $H^1(\mathcal{M})$ the exact *LB* spectrum. However, this space is infinite dimensional and cannot be treated numerically, even in the weak form shown in Eq. (23). One then needs to set up an approximation scheme by building a sequence $\{\mathcal{V}_r\}_{r=0}^{\infty}$ of finite-dimensional subspaces of H^1 with increasing dimension such that in the limit one recovers the full space $\lim_{r\to\infty} \mathcal{V}_r \to H^1$. Accordingly, the approximate eigenvectors on $f_n^{(r)}$ and eigenvalues $\lambda_n^{(r)}$ would converge, in the limit $r \to \infty$ to the exact LB eigenvectors and eigenvalues of the infinite-dimensional problem (23) in H^1 . In practice, chosen a finite set of basis functions $\left\{\phi_i^{(r)}\right\}_{i=1,\ldots,N_r}$ for the subspace $\mathcal{V}_r$, any function $f \in H^1$ can approximated as

上式左侧已经过分部积分处理。测试函数 ϕ 可属于不同函数类，但对于拉普拉斯-贝尔特拉米特征值问题，通常选取索伯列夫空间 $H^1(\mathcal{M})$ (即 H^1)，该空间定义为所有存在弱一阶导数的 L^2 函数构成的空间，此时问题是适定的，且已证明解存在。需要强调的是，对于分段线性流形 $\mathcal{M}$ ，索伯列夫空间 $H^1(\mathcal{M})$ 包含流形整个定义域上的所有函数，即不仅包含顶点或单形中心，也包含平直单形的内部。下文我们将函数空间 $H^1(\mathcal{M})$ 上拉普拉斯-贝尔特拉米算子的谱称为精确 LB 谱。但该空间是无限维的，即使是式 (23) 所示的弱形式也无法进行数值处理，因此需要建立近似框架: 构造一个维数递增的 H^1 有限维子空间序列 $\{\mathcal{V}_r\}_{r=0}^{\infty}$ ，使得在极限下可以得到完整空间 $\lim_{r\to\infty}\mathcal{V}_r \to H^1$ 。相应地，$f_n^{(r)}$ 上的近似特征向量和近似特征值 $\lambda_n^{(r)}$ 会在极限 $r\to\infty$ 下收敛到 H^1 中无限维问题 (23) 的精确拉普拉斯-贝尔特拉米特征向量与特征值。实际操作中，当选定子空间 $\mathcal{V}_r$ 的一组基函数 $\left\{\phi_i^{(r)}\right\}_{i=1,\ldots,N_r}$ 后，任意函数 $f\in H^1$ 都可以近似表示为

$$f(\mathbf{x}) = \sum_{i=1}^{N} c_i \phi_i(\mathbf{x}). \tag{24}$$

With this expansion, and the basis used as test functions, Eq. (23) can be rewritten in the form of a finite-dimensional generalized eigenvalue problem:

通过上述展开，并将基函数用作测试函数，式 (23) 可以改写为有限维广义特征值问题的形式:

$$L\vec{c} = \lambda M\vec{c} \tag{25}$$

where we have introduced the two matrices L and M with matrix elements

其中我们引入了两个矩阵 L 和 M ，它们的矩阵元素为

$$L_{i,j} \equiv \int_{\mathcal{M}} d^d\mathbf{x}\vec{\nabla}\phi_i(x)\cdot\vec{\nabla}\phi_j(x), \tag{26}$$

$$M_{i,j} \equiv \int_{\mathcal{M}} d^d\mathbf{x}\phi_i(x)\phi_j(x). \tag{27}$$

For the specific class of FEM we considered, the procedure of building a consistent sequence of subspaces is called refinement, and it allows extrapolating the result of solutions of the approximate LB eigenproblem on a finite set of subspaces $\mathcal{V}_r$ to the infinite refinement level r limit, which corresponds to H^1 . The results discussed in the following are obtained from an extrapolation to infinite refinement level. The reader can find a detailed technical discussion about the refinement construction and extrapolation in Ref. [22]. The main point of the FEM discretization of the LB operator is actually the fact that it allows one to extract, by extrapolation, an arbitrarily good approximation to the result of the eigenproblem on the full infinite-dimensional Sobolev space of functions H^1 on the piecewise flat manifold under investigation. Of course, while powerful, this approach is certainly not numerically cheap. However, we think it is useful in order to check how much results obtained with other discretizations of the LB operator deviate from the exact spectrum and eigenfunctions, as we discuss in the next section.

对于我们研究的这类有限元方法，构造一致子空间序列的过程称为加密，它允许我们将有限个子空间 $\mathcal{V}_r$ 上近似拉普拉斯-贝尔特拉米特征值问题的求解结果外推到无限加密水平 r 的极限，该极限对应 H^1 。下文讨论的所有结果均是外推到无限加密水平后得到的。读者可以在文献 [22] 中找到关于加密构造和外推的详细技术讨论。有限元方法离散拉普拉斯-贝尔特拉米算子的核心优势在于，它可以通过外推得到我们研究的分段平直流形上全无限维索伯列夫函数空间 H^1 中特征值问题的任意精度近似。当然，这种方法虽然能力强大，但其计算成本并不低。不过我们认为，该方法对于检验其他拉普拉斯-贝尔特拉米算子离散方法得到的结果与精确谱、精确特征函数的偏离程度是很有帮助的，我们将在下一节讨论相关内容。

Numerical Results

数值结果

Here, we show a comparison between the few smallest eigenvalues of the LB operator acting on the Sobolev space of functions H^1 for CDT slices, accessed through FEM, and the results of the dual graph discretization of the LB operator, as described in section "Graph Discretization of the Laplace-Beltrami Operator". The effective dimension obtained with the two methods is investigated in Ref. [22] for slices in two points in the phase diagram. For example, for $(k_0, \Delta) = (0.75, 0.7)$, the best effective dimension estimate via FEM suggests a value $d_{EFF}^{(FEM)} = 2.088\,(18)$, which is in contrast with the value $d_{EFF}^{(DG)} \simeq 1.6$ as found in Ref. [14]. For the sake of comparison, we show here how the estimate of the critical index of the $C_b - C_{dS}$ transition along the line $k_0 = 0.75$ differs from the one computed using dual graph methods, which has been discussed in section "Bifurcation Phase and $C_b - C_{dS}$ Phase Transition".

在此，我们展示了通过有限元方法得到的、作用于 CDT 切片 Sobolev 函数空间 H^1 上的拉普拉斯-贝尔特拉米 (LB) 算子的若干最小特征值，与" 拉普拉斯-贝尔特拉米算子的图离散化" 一节中所述 LB 算子对偶图离散化结果的对比。文献 [22] 已经研究了相图中两个点处的切片用两种方法得到的有效维度。例如，对于 $(k_0, \Delta) = (0.75, 0.7)$ ，通过有限元方法得到的最优有效维度估计值为 $d_{EFF}^{(FEM)} = 2.088\,(18)$ ，这与文献 [14] 中得到的 $d_{EFF}^{(DG)} \simeq 1.6$ 不一致。为便于比较，我们在此展示沿 $k_0 = 0.75$ 线的 $C_b - C_{dS}$ 相变临界指数估计，与使用对偶图方法计算得到的结果有何差异，后者已在" 分岔相与 $C_b - C_{dS}$ 相变" 一节中讨论。

In order to extract results useful for the continuum limit, the following three limiting procedures should be performed:

为了提取对连续极限有用的结果，需要执行以下三种极限步骤:

1. For each simplicial manifold $\mathcal{M}$, one has to extrapolate the individual FEM eigenvalues to "infinite refinement level" $\lambda_n^{(r)}[\mathcal{M}] \xrightarrow{r\to\infty} \lambda_n^{(\infty)}[\mathcal{M}]$, in order to obtain an accurate enough approximation of the spectrum of the exact LB differential operator on $\mathcal{M}$ (see Ref. [22] for details about this step).

1. 对于每个单纯流形 $\mathcal{M}$ ，必须将单个有限元特征值外推到" 无限精修水平" $\lambda_n^{(r)}[\mathcal{M}] \xrightarrow{r\to\infty} \lambda_n^{(\infty)}[\mathcal{M}]$ ，从而得到 $\mathcal{M}$ 上精确 LB 微分算子谱足够准确的近似 (关于这一步的细节见文献 [22])。

2. For each ensemble of configurations at specific values of the parameters, one should first perform

an average of the eigenvalues at each specific order n and then take the thermodynamic limit (i.e., infinite volumes in lattice units) $\langle\lambda_n\rangle_V \equiv \frac{1}{|\mathcal{C}_V|}\sum_{\mathcal{M}\in\mathcal{C}_V}\lambda_n^{(\infty)}[\mathcal{M}] \xrightarrow{V\to\infty} \langle\lambda_n\rangle_\infty$ by considering the spectra of ensembles $\mathcal{C}_V$ with increasing volumes.

2. 对于参数取特定值的每组构型系综,应当先对每个特定阶 n 的特征值求平均,再通过研究体积逐渐增大的系综 $\mathcal{C}_V$ 取热力学极限 (即格点单位下的无限体积) $\langle\lambda_n\rangle_V \equiv \frac{1}{|\mathcal{C}_V|}\sum_{\mathcal{M}\in\mathcal{C}_V}\lambda_n^{(\infty)}[\mathcal{M}] \xrightarrow{V\to\infty} \langle\lambda_n\rangle_\infty$ 。

3. Finally, one can study the critical scaling of the twice-extrapolated eigenvalues $\langle\lambda_n\rangle_\infty(k_0,\Delta)$ observed as the phase transition is approached and match it with the shifted power law expressed by Eq. (21).

3. 最后，当趋近相变点时，可以研究经过两次外推的特征值 $\langle\lambda_n\rangle_\infty(k_0,\Delta)$ 的临界标度，并将其与式 (21) 给出的平移幂律进行匹配。

In the rest of this section, we considered only some points along the line $k_0 = 0.75$ and the critical scaling of the first ten orders of eigenvalues. First, we have to possibly extrapolate to infinite refinement level, and then, we can perform the thermodynamic limit ($V_S \to \infty$) order by order. For this second step, in general, we do not have a precise expectation on the large-scale behavior for the eigenvalues of gapped slices, but we followed [28] and used the simplest form compatible with data, that is, a quadratic polynomial in $1/V_S$:

在本节剩余部分，我们仅考虑沿 $k_0 = =0.75$ 线的若干点，以及前 10 阶特征值的临界标度。首先，我们需要先外推到无限精修水平，随后再逐阶进行热力学极限 ($V_S \to \infty$) 。对于第二步，一般来说我们无法预先知道有能隙切片特征值的大尺度行为，因此我们遵循文献 [28]，采用与数据相容的最简单形式，即关于 $1/V_S$ 的二次多项式:

$$\langle\lambda_n\rangle_V = \langle\lambda_n\rangle_\infty + \frac{A_n}{V_S} + \frac{B_n}{V_S^2}. \tag{28}$$

The thermodynamical limit consists then of fitting data with Eq. (28) in order to extract the possibly nonzero constant terms $\langle\lambda_n\rangle_\infty$, order by order in n .

热力学极限即为用式 (28) 拟合数据，从而逐阶在 n 中提取可能不为零的常数项 $\langle\lambda_n\rangle_\infty$ 。

For every point in the phase diagram and every order n taken into account, the thermodynamic limit extrapolations yielded $\chi^2/dof < 1$. For illustration purposes, Fig. 8 displays the extrapolation to the thermodynamic limit for the first ten eigenvalue orders in the phase space point $k_0 = 0.75, \Delta = 0.575$.

对于相图中的每个点以及考虑的每一阶 n , 热力学极限外推都得到了 $\chi^2/dof < 1$ 。为便于说明，图 8 展示了相空间点 $k_0 = 0.75, \Delta = 0.575$ 中前十阶本征值的热力学极限外推结果。

We then analyzed the first ten eigenvalue orders by fitting our data with the shifted power law in Eq. (21), imposing a common critical index υ and critical point Δ_{crit} for every order n , as observed also for the dual graph case discussed in section "Bifurcation Phase and $C_b - C_{dS}$ Phase Transition". We used data coming from eight phase space points with Δ ranging from 0.45 to 0.625 we chose not to go too deep inside C_b phase because of the influence of the expected subdominant terms of the critical scaling and excluded them by checking the stability of our estimate of υ under the removal of the points with lower Δ parameter. We obtained, as best-fit

parameters $\upsilon = 0.293\,(10)$ (recall that $\upsilon^{(DG)} = 0.55\,(4)$ in section "Bifurcation Phase and $C_b - C_{dS}$ Phase Transition" at the same value of k_0) and $\Delta_{\text{crit}} = 0.6316\,(15)$, with reduced chi-squared $\frac{\chi^2}{\text{dof}} = \frac{67}{68} \simeq 1$. Data and best-fit curves for each order up to $n_{\max} = 10$ are displayed in Fig. 9.

随后我们对前十阶本征值进行了分析，使用式 (21) 中的偏移幂律拟合数据，和“分岔相与 $C_b - C_{dS}$ 相变”一节讨论的对偶图情况一致，我们对每一阶 n 都施加了相同的临界指数 υ 和临界点 Δ_{crit} 。我们使用了八个相空间点的数据，其中 Δ 的范围为 0.45 至 0.625: 由于临界标度预期次主导项的影响，我们选择不深入 C_b 相内部，并且通过移除 Δ 参数更小的点后检验 υ 估计值的稳定性，将这些点排除。我们最终得到的最佳拟合参数为 $\upsilon = 0.293\,(10)$ (还记得“分岔相与 $C_b - C_{dS}$ 相变”一节中相同 k_0 取值下的 $\upsilon^{(DG)} = 0.55\,(4)$ 吗) 和 $\Delta_{\text{crit}} = 0.6316\,(15)$ ，约化卡方为 $\frac{\chi^2}{\text{dof}} = \frac{67}{68} \simeq 1$ 。最高到 $n_{\max} = 10$ 阶的各阶数据与最佳拟合曲线展示在图 9 中。

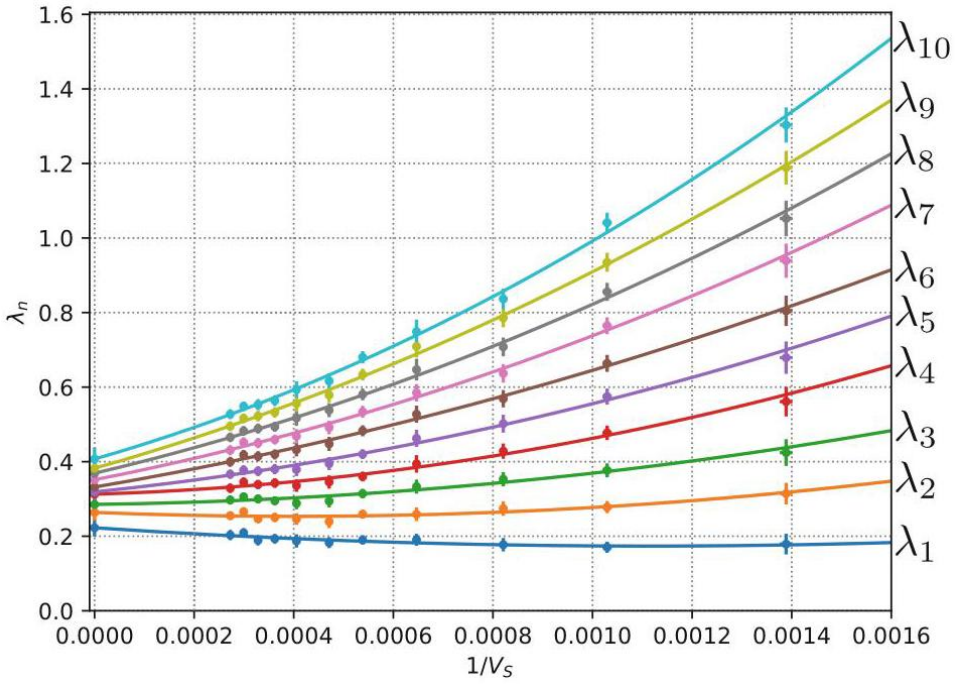

Fig. 8 First ten eigenvalue orders of spatial slices (with $V_S > 500$) vs $1/V_S$, with extrapolation to the thermodynamic limit ($V_S \to \infty$) in C_b phase. Phase space point $(k_0, \Delta) = (0.75, 0.7)$, total spatial volume $V_{S,\text{tot}} = 80$ k

图 8 空间切片的前十阶本征值 (含 $V_S > 500$) 与 $1/V_S$ 的关系，以及 C_b 相中的热力学极限外推 ($V_S \to \infty$) 。相空间点 $(k_0, \Delta) = (0.75, 0.7)$ ，总空间体积 $V_{S,\text{tot}} = 80$ k

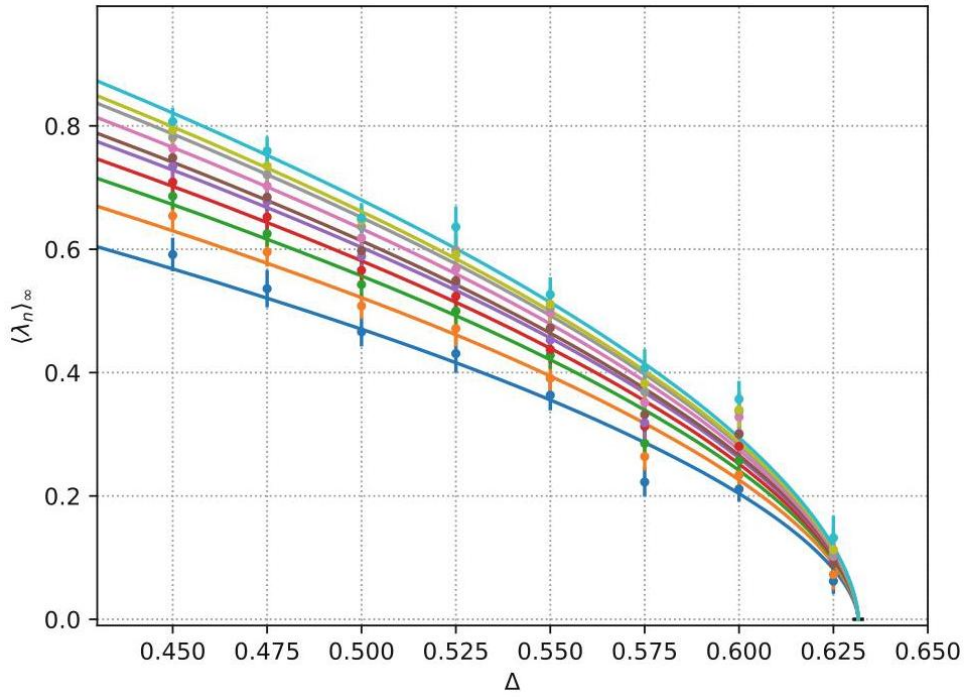

Fig. 9 Critical behavior of the first ten eigenvalue orders along the line at fixed $k_0 = 0.75$ and varying Δ, with best-fit curves of the form shown in Eq. (21) with common v and Δ_{crit}. Curves of increasing eigenvalue order are shown from below to above in the plot

图 9 固定 $k_0 = 0.75$ 改变 Δ 时，沿该直线前十阶本征值的临界行为，带有带有相同 v 和 Δ_{crit}、形式如式 (21) 的最佳拟合曲线。图中从下到上依次为本征值阶数递增的曲线

In conclusion, it is apparent that data are still qualitatively compatible with the critical scaling from dual graph spectra discussed in section "Bifurcation Phase and $C_b - C_{dS}$ Phase Transition" and based on [28], but, while the location of the transition line agrees with those results, the values found for the critical indexes appear significantly different than the previous estimates. Such a difference might be important in assessing the quality of estimates based on graph discretization, in particular, if critical indexes of different observables have to be compared to find a physical continuum limit in the phase diagram.

总而言之，显然数据在定性上仍然与“分岔相与 $C_b - C_{dS}$ 相变”一节中讨论的、基于文献 [28] 得到的对偶图谱临界标度相容，但尽管相变线的位置与已有结果一致，我们得到的临界指数值与之前的估计存在显著差异。这种差异对于评估基于图离散化的估计质量可能十分重要，尤其是当需要比较不同可观测量的临界指数，以在相图中找到具有物理意义的连续极限时。

Gauge Fields on Fluctuating Geometries

涨落几何上的规范场

The study of dynamical triangulations in the presence of additional quantum fields has been considered frequently in the literature. This is quite natural: if CDT will reveal a successful way to quantize QG, it should

eventually be considered in connection with other interacting fields; on the other hand, the presence of other fields may by itself enter the analysis of the renormalization group flow and the search for the continuum limit.

文献中已频繁研究存在额外量子场情况下的动力学三角剖分问题。这十分自然: 如果因果动力学三角剖分 (CDT) 能成功实现量子引力 (QG) 的量子化，它最终必然要和其他相互作用场结合讨论；另一方面，其他场的存在本身就会影响重整化群流分析以及连续极限的搜寻。

Abelian and non-Abelian gauge fields are a notable case, given their role in the formulation of the standard model. A first important aspect concerns the way the local gauge symmetry and the gauge fields are implemented in the context of dynamical triangulations. Gauge fields in a discrete setting, e.g., a hypercubic lattice, are usually described [30] in terms of elementary parallel transporters living on lattice links (gauge link variables), which permit to translate the local frame choice for the internal symmetry group from one lattice site to the other. Therefore, local gauge transformations act on lattice sites, which is the same place where matter fields live.

鉴于阿贝尔和非阿贝尔规范场在标准模型构建中的核心作用，它们是十分值得关注的研究案例。第一个重要问题是，如何在动力学三角剖分的框架下实现局部规范对称性和规范场。在离散环境 (例如超立方格点) 中，规范场通常 [30] 用位于格点键上的基本平行移动算子 (规范链接变量) 描述，通过这类算子可以将内部对称性群的局部规范架选择从一个格点传递到另一个格点。因此，局部规范变换作用在格点上，这和物质场所处的位置一致。

In the context of dynamical triangulations, it is most natural instead to make the choice for the internal symmetry consistent with that for the Lorentz symmetry, i.e., to associate gauge transformations to the simplices composing the triangulations. In this way, the elementary parallel transports are associated with the links of the dual graph, which connect adjacent simplices and are dual to the hypersurfaces separating them.

而在动力学三角剖分的框架下, 最自然的选择是让内部对称性的选取和洛伦兹对称性的选取保持一致，也就是将规范变换关联到构成三角剖分的单形上。按照这种选取，基本平行移动算子关联到对偶图的边，这些边连接相邻单形，对偶于分隔相邻单形的超曲面。

Once the nature of gauge transformations and gauge fields on the triangulation has been clarified, the first task is to write down a properly discretized action for the composite gravity-gauge system. In the following, $\mathcal{C}_G(\mathcal{T})$ will stand for the space of all possible gauge field configurations on the triangulation $\mathcal{T}$, where G is the gauge group. The action can be formally decomposed, in the minimal coupling paradigm, as $S[\Phi, \mathcal{T}] = S_{CDT}[\mathcal{T}] + S_{\mathrm{YM}}[\Phi; \mathcal{T}]$, with $\Phi \in \mathcal{C}_G(\mathcal{T})$ and where S_{YM} represents the minimally coupled gauge action in the gravity background $\mathcal{T}$. The specific form of S_{YM}, which correctly represents Yang-Mills theory in the continuum limit, can be easily built taking as a guide what is usually done on a standard hypercubic lattice [30], as we discuss in more detail in the following.

明确三角剖分上规范变换和规范场的性质后，首要任务就是为引力-规范复合系统写出恰当的离散化作用量。下文将用 $\mathcal{C}_G(\mathcal{T})$ 表示三角剖分 $\mathcal{T}$ 上所有可能规范场构型的空间，其中 G 为规范群。在最小耦合范式下，作用量可以形式分解为 $S[\Phi,\mathcal{T}]=S_{CDT}[\mathcal{T}]+S_{\mathrm{YM}}[\Phi;\mathcal{T}]$，其中 $\Phi\in\mathcal{C}_G(\mathcal{T})$，$S_{\mathrm{YM}}$ 代表引力背景 $\mathcal{T}$ 下的最小耦合规范作用量。正如我们下文会详细讨论的，只要以标准超立方格点上的常规构造方法 [30] 为参考，就可以轻松得到能在连续极限下正确描述杨-米尔斯理论的 S_{YM} 具体形式。

Yang-Mills Action Coupled to Dynamical Triangulations

耦合到动态三角剖分的杨-米尔斯作用量

Continuum Yang-Mills (YM) theories are described in terms of the gauge field $A_\mu=A_\mu^a T^a$, where T^a are the generators of the Lie algebra $\left(a\in\{1,\ldots,N^2-1\}\right.$ for $SU(N)$, normalized as $\mathrm{Tr}(T_aT_b)=\delta_{ab}/2$), while the continuum action in flat Euclidean space reads

连续杨-米尔斯 (YM) 理论由规范场 $A_\mu=A_\mu^aT^a$ 描述，其中 T^a 是李代数 $\left(a\in\{1,\ldots,N^2-1\}\right.$ 对应 $SU(N)$ 的生成元，归一化为 $\mathrm{Tr}(T_aT_b)=\delta_{ab}/2$ ），平坦欧几里得空间中的连续作用量为

$$S_{\mathrm{YM}}=\frac{1}{4}\int_{\mathcal{M}}d^dxF^a_{\mu\nu}F^{a\mu\nu}, \tag{29}$$

where $F^a_{\mu\nu}=\partial_\mu A^a_\nu-\partial_\nu A^a_\mu+gf^{abc}A^b_\mu A^c_\nu$. A minimal coupling to gravity (described in terms of the Einstein-Hilbert action) leads to the following modification:

其中 $F^a_{\mu\nu}=\partial_\mu A^a_\nu-\partial_\nu A^a_\mu+gf^{abc}A^b_\mu A^c_\nu$ 。与引力 (以爱因斯坦-希尔伯特作用量描述) 的最小耦合导出如下修正形式:

$$S_{\mathrm{YM+EH}}=\int_{\mathcal{M}}d^dx\sqrt{-g}\left[\frac{1}{4}F^a_{\mu\nu}F^{a\mu\nu}+(R-2\Lambda)\right], \tag{30}$$

where g in $\sqrt{-g}$ stands now for the determinant of the metric tensor, R is the scalar curvature, and Λ is the cosmological constant.

其中 g 在 $\sqrt{-g}$ 中现在代表度规张量的行列式，R 是标量曲率，Λ 是宇宙学常数。

In flat space-time, YM theories are usually discretized on a hypercubic lattice in terms of link variables $U_\mu(n)$, representing the elementary parallel transporters from lattice site n to lattice site $n+\hat{\mu}$ and taking values in the gauge group G . Local gauge transformations $g(n)$ act on lattice sites, and gauge link variables transform as $U_\mu(n)\to g(n)U_\mu(n)g^{-1}(n+\hat{\mu})$. The standard and simplest gauge-invariant discretization of the action is given in terms of the so-called plaquette operator (plaquette or Wilson action):

在平坦时空中，杨-米尔斯理论通常在超立方格点上用链接变量 $U_\mu(n)$ 离散化，$U_\mu(n)$ 代表从格点 n 到格点 $n+\hat{\mu}$ 的基本平行移动算子，取值于规范群 G 。局域规范变换 $g(n)$ 作用在格点上，规范链接变量按 $U_\mu(n)\to g(n)U_\mu(n)g^{-1}(n+\hat{\mu})$ 变换。作用量最标准、最简的规范不变离散化由所谓的 plaque 算子给出 (plaque 作用量或威尔逊作用量):

$$S_{\mathrm{YM}} \equiv -\frac{2N}{g^2} \sum_{\square} \left[\frac{1}{N} \operatorname{Re} \operatorname{Tr} \Pi_{\square} - 1 \right], \tag{31}$$

where $\Pi_{\square}$ stands for the oriented product of gauge link variables around an elementary plaquette $\square$, and the sum extends over all possible plaquettes (For the Abelian gauge group $U(1)$, the factor $2N/g^2$ is substituted by $1/g^2$.). The fact that Eq. (31) correctly reproduces continuum YM in the naïve continuum limit follows from the second-order expansion of the correspondence between plaquettes and continuum field strengths, $\Pi_{\mu\nu} \simeq \exp\left(iga^2 F_{\mu\nu}\right)$, where $\mu\nu$ fixes the plaquette orientations and a is the lattice spacing, which in turn derives from the correspondence $U_{\mu} \simeq \exp\left(igaA_{\mu}\right)$.

其中 $\Pi_{\square}$ 代表基本 plaque $\square$ 周边规范链接变量的定向乘积，求和遍历所有可能的 plaquette(对于阿贝尔规范群 $U(1)$，因子 $2N/g^2$ 替换为 $1/g^2$)。式 (31) 能在朴素连续极限下正确重现连续杨-米尔斯理论，这源于 plaque 与连续场强度对应关系的二阶展开 $\Pi_{\mu\nu} \simeq \exp\left(iga^2 F_{\mu\nu}\right)$，其中 $\mu\nu$ 固定 plaque 取向，a 是格距，这又反过来源自对应关系 $U_{\mu} \simeq \exp\left(igaA_{\mu}\right)$。

On a triangulated, curved space-time instead, as already explained above, we consider a formulation where elementary parallel transporters are associated with dual links connecting pairs of adjacent simplices. In the following, such variables will be indicated as $U_{\mu}(s)$, where s stands for a particular simplex and μ is the dual link direction, or simply as U_l, where l is the dual link joining two simplices s and s'; under a local gauge transformation $g(s)$, $U_l \to g(s) U_l g^{-1}(s')$. All dual links connect ideally the centers of the simplices, so they all have equal lengths, except when simplices are anisotropic, as usual in 4D CDT. Gauge-invariant objects are associated with traces of closed loops over the dual graph, and, in analogy with the standard formulation, we will call plaquette the most elementary closed loop, as well as the gauge-invariant operator associated with it. A plaquette encloses an elementary 2D surface of the dual graph, which is dual to a $(d-2)$ simplex of the original triangulation, i.e., a bone in the Regge terminology [31]: this is the geometrical object where space-time curvature resides; now, it becomes the object where the gauge curvature lives as well.

而在三角化的弯曲时空中，正如前文所述，我们采用的表述是: 基本平行输运子关联连接相邻单形对的对偶链。下文里，这类变量记为 $U_{\mu}(s)$，其中 s 代表特定单形，μ 是对偶链方向，也可简记为 U_l，其中 l 是连接两个单形 s 和 s' 的对偶链；在局部规范变换下满足 $g(s), U_l \to g(s) U_l g^{-1}(s')$。所有对偶链理想情况下连接单形中心，因此长度均相等——4D 因果动力学三角剖分 (CDT) 中各向异性单形是例外，这符合常规。规范不变量对应对偶图上闭回路的迹，类比标准表述，我们将最基本的闭回路及其关联的规范不变算符都称为面元 (plaquette)。一个面元围出对偶图的一块基本二维曲面，它对偶于原三角剖分的 $(d-2)$ 单形，也就是里奇术语中的骨 (bone)[31]: 时空曲率就定域在这个几何对象上；现在，规范曲率也定域在这个对象上。

A plaquette Π_b corresponds to the ordered product of n_b dual link variables going around bone b, where n_b is the coordination number of the bone. The area enclosed by an elementary plaquette is An_b, where A is the elementary unit of area (e.g., one third of the simplex area in two dimensions), so that the correspondence between plaquettes and continuum field strengths reads

<text id="1"> 一个面元 Π_b 对应绕骨 b 的 n_b 个对偶链变量的有序乘积，其中 n_b 是该骨的配位数。基本面元围出的面积为 An_b，其中 A 是基本面积单位 (例如二维中单形面积的三分之一)，因此面元与连续场强的对应关系为:

$$\Pi_b \simeq \exp\left(ign_b A F_{\mu\upsilon}\right) \tag{32}$$

where μ and υ define the plane orthogonal to the bone. The second-order expansion of the trace of the plaquette returns $F^2_{\mu\nu}$ also in this case, however accompanied by a factor n_b^2 which, contrary to what happens on a lattice with a fixed and homogeneous geometry, is a dynamical variable that must be properly taken care of.

其中 μ 和 υ 确定了垂直于骨的平面。本例中面元迹的二阶展开同样给出 $F^2_{\mu\nu}$，但附带了因子 n_b^2；和固定均匀几何格点的情况不同，这个因子是动力学变量，需要做适当处理。

In order to understand how, let us consider that, in the continuum action, $F^2_{\mu\nu}$ gets multiplied by $d^dx\sqrt{-g}$ factor, which measures the physical volume. If we want to count volume while summing over bones, we have to take into account the volume pertaining to each bone, which is proportional (times a constant geometrical factor for isotropic simplices) to the number of simplices sharing the bone, i.e., to the coordination number n_b . From this reasoning, it is clear that, since the second-order expansion of the plaquette returns $F^2_{\mu\nu}$ with a n_b^2 factor attached, one needs to divide by n_b the contribution from each plaquette and then sum over all plaquettes. The form of the plaquette action over a triangulation $\mathcal{T}$ then reads

为了说明处理方式，我们注意到连续作用量中 $F^2_{\mu\nu}$ 会乘上测量物理体积的 $d^dx\sqrt{-g}$ 因子。如果我们要在对所有骨求和时统计体积，就必须考虑每个骨对应的体积: 对于各向同性单形，该体积正比于共享该骨的单形数量，也就是配位数 n_b (相差一个常数几何因子)。由此不难看出，由于面元的二阶展开给出附带 n_b^2 因子的 $F^2_{\mu\nu}$，我们需要将每个面元的贡献除以 n_b，再对所有面元求和。于是三角剖分 $\mathcal{T}$ 上面元作用量的形式为:

$$S_{\mathrm{YM}} \equiv -\beta \sum_{b\in\mathcal{T}^{(d-2)}} \frac{\widetilde{\Pi}_b}{n_b}, \tag{33}$$

where we adopted the shorthand $\widetilde{\Pi}_b \equiv \left[\frac{1}{N}\,\mathrm{Re}\,\mathrm{Tr}\,\Pi_b - 1\right]$, $\mathcal{T}^{(d-2)}$ is the set of all bones of the triangulation $\mathcal{T}$, while β denotes, as usual, the inverse gauge coupling proportional to $1/g^2$. This expression is valid for any dimension d ; however, the exact definition of β includes geometrical factors (like the elementary area A and the simplex volume) which depend on d .

其中我们采用简写 $\widetilde{\Pi}_b \equiv \left[\frac{1}{N}\,\mathrm{Re}\,\mathrm{Tr}\,\Pi_b - 1\right]$, $\mathcal{T}^{(d-2)}$ 是三角剖分 $\mathcal{T}$ 所有骨的集合，β 按惯例表示正比于 $1/g^2$ 的逆规范耦合。该表达式对任意维数 d 都成立；不过 β 的精确定义包含依赖于 d 的几何因子 (例如基本面积 A 和单形体积)。

In the following, we will consider an explicit realization of the above formulation in two space-time dimensions. In this case, the gravity sector becomes particularly simple: the curvature term depends only on the global topology of the manifold (Gauss-Bonnet theorem), which is usually kept fixed, so it can be ignored and the cosmological constant term is the only nontrivial coupling. In particular, the pure-gravity contribution for CDT action in Euclidean space-time reads [32]

下文我们将考虑上述公式在二维时空下的显式实现。这种情况下，引力部分变得格外简单: 曲率项仅依赖流形的整体拓扑 (高斯-博内定理)，而该拓扑通常保持固定，因此曲率项可以忽略，仅宇宙学常数项是非平凡耦合。具体而言，欧几里得时空中 CDT 作用量的纯引力贡献为 [32]

$$S_{\mathrm{CDT}}^{(2\mathrm{D})}[\mathcal{T}] = \lambda N_2[\mathcal{T}], \tag{34}$$

where $N_2[\mathcal{T}]$ is the number of simplices (triangles) in $\mathcal{T}$ and λ is the only coupling, related to the cosmological constant. When considering the integral over all possible triangulations weighted by $\exp\left(-S_{\mathrm{CDT}}^{(2\mathrm{D})}[\mathcal{T}]\right)$, a critical behavior is observed as $\lambda \to \lambda_c = \log 2$; in particular, both the average total volume and the correlation length for foliation volumes diverge as $\lambda \to \lambda_c$ from above.

其中 $N_2[\mathcal{T}]$ 是 $\mathcal{T}$ 中单纯形 (三角形) 的数量，λ 是唯一与宇宙学常数相关的耦合。当我们对以 $\exp\left(-S_{\mathrm{CDT}}^{(2\mathrm{D})}[\mathcal{T}]\right)$ 加权的所有可能三角剖分做积分时，在 $\lambda \to \lambda_c = \log 2$ 处观察到临界行为；具体来说，平均总体积和叶状体积的关联长度都在 $\lambda \to \lambda_c$ 从上方趋近临界点时发散。

In Fig. 10, we show an explicit realization of a configuration of gauge link variables $U_\mu(s)$ living on a 2D causal triangulation and of a plaquette built with them. In this case, μ is either spatial or temporal, with positive orientations taken rightward in space and upward in time; each simplex is associated with one temporal link (either ingoing or outgoing) and two spatial links (one ingoing and one outgoing). In the particular example of plaquette shown in the figure, we have $n_b = 6$, which corresponds to a locally flat space-time (while $n_b > 6$ and $n_b < 6$ correspond, respectively, to negative and positive local curvature).

图 10 展示了规范链接变量 $U_\mu(s)$ 在二维因果三角剖分上的具体构型，以及由这些链接构造的格块。在该情形中，μ 链接要么类空要么类时，规定正方向为空间向右、时间向上；每个单纯形对应一个时间链接 (入射或出射) 和两个空间链接 (一个入射、一个出射)。图中所示格块的具体例子为 $n_b = 6$，对应局域平坦时空 (而 $n_b > 6$ 和 $n_b < 6$ 分别对应负局域曲率和正局域曲率)。

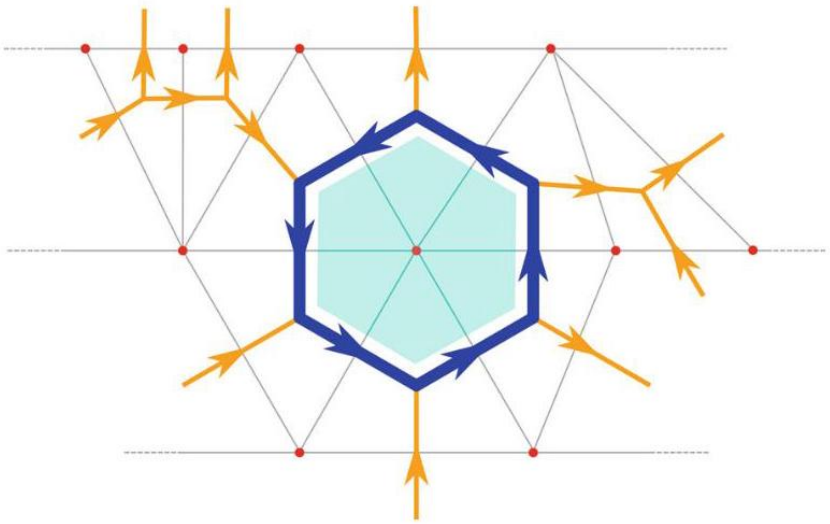

Fig. 10 Sketch of a plaquette operator on a typical 2D CDT triangulation. We have considered a plaquette built around a vertex with $n_b = 6$, corresponding to zero curvature. The direction of gauge links (apart from those belonging to the plaquette) has been drawn according to the convention adopted in the text, i.e., from bottom to up and from left to right. All triangles in this and the following figures should be considered as equilateral, even if they are necessarily drawn differently

图 10 典型二维 CDT 三角剖分上的格块算符示意图。我们构造的格块环绕一个顶点数为 $n_b = 6$ 的顶点，对应零曲率。除格块自身包含的链接外，所有规范链接的方向均按照文中约定绘制，即自下而上、从左到右。本图及后续图中所有三角形实际都应视为等边三角形，仅因绘图需求做了调整

Numerical Simulations of CDT Coupled to YM Theories

耦合杨-米尔斯理论的因果动态三角剖分数值模拟

A Monte Carlo approach to the computation of path integral averages requires to sample the possible triangulation+gauge field configurations according to their weight, $\exp\left(-S_{\mathrm{CDT}}^{(2\mathrm{D})} - S_{\mathrm{YM}}\right)$, with S_{YM} defined in Eq. (33). In order to that, one has to devise a set of Markov chain moves which guarantee detailed balance, ergodicity, and aperiodicity. Since the action is local, the natural choice is to look for a set of local moves, which change the triangulation and/or the gauge configuration only locally. Moreover, it seems convenient to think of moves which change alternatively either the gauge field or the triangulation, so that one can try to implement standard algorithms already used either for lattice gauge theories or for CDT.

计算路径积分平均的蒙特卡洛方法需要根据权重对可能的三角剖分 + 规范场构型进行采样，即 $\exp\left(-S_{\mathrm{CDT}}^{(2\mathrm{D})} - S_{\mathrm{YM}}\right)$，其中 S_{YM} 由式 (33) 定义。为实现这一点，必须设计一组马尔可夫链移动，以满足细致平衡、各态历经性和非周期性要求。由于作用量是定域的，自然会选择一组定域移动，它们仅在局部改变三角剖分和/或规范构型。此外，采用交替改变规范场或三角剖分的移动方案似乎更为方便，这样我们就可以直接应用已分别用于格点规范理论或 CDT 的标准算法。

However, while this idea works smoothly for updating gauge configurations, moves regarding the triangulation present some additional difficulties. Indeed, any change in the space-time geometry modifies the gauge connection as well: some simplices are added/destroyed or differently glued with the rest of the triangulation, implying a modification of the dual graph and of the gauge link variables living on it. Therefore, one can refer to standard CDT moves (for a review, see Ref. [32]); however, a proper modification must be devised, involving a certain number of gauge links which are added/destroyed or differently connected with the rest of the gauge configuration: as the number of space-time dimensions increases, the number of link variables involved in each CDT move increases, making the task less and less trivial. Partial local gauge fixing can help reducing the number of nontrivial link variables involved and in fact permits to construct a viable algorithm in two dimensions, which is the case more deeply discussed in the following.

然而，这一思路在更新规范组态时运行顺畅，但三角剖分相关移动存在不少额外困难。事实上，时空几何的任何改变都会同时修改规范联络: 部分单纯形被添加/移除，或与三角剖分的其余部分以不同方式粘合，这意味着其对偶图以及其上的规范链接变量都会发生改变。因此，我们可以参考标准 CDT 移动 (综述见文献 [32])，但必须设计合适的修改方案，处理添加/移除，或是以不同方式连接到其余规范组态的若干规范链接: 随着时空维数增加，每次 CDT 移动涉及的链接变量数量也会增加，导致这项任务越来越复杂。部分定域规范固定可以帮助减少涉及的非平庸链接变量数量，实际上它能够在二维情况下构造出可行的算法，二维也是下文深入讨论的情形。

Algorithm for 2D CDT

二维因果动态三角剖分 (CDT) 算法

The algorithm usually adopted in pure-gravity CDT simulations is a local Metropolis-Hastings (It is interesting to notice that dynamical triangulation is one of the cases where the Hastings variant of the original Metropolis algorithm is actually needed. Indeed, since the move modifies the space of stochastic variables, selection probabilities for the move and for its inverse in general differ, so that their ratio contributes to the acceptance step.) algorithm [33, 34], based on a set of moves that need to preserve the causal structure of the triangulation, i.e., that change the triangulation without spoiling its foliation; a proper set is provided by the so-called Alexander moves [35, 36] . In two dimensions, the set consists of just three moves, usually denoted as $(2,2)$, $(2,4)$, and $(4,2)$, to specify the number of simplices involved before and after the move. In the following, we provide a brief description of such moves and discuss how they must be modified in order to take into account the corresponding modification of the gauge configuration. A more detailed discussion and a proof of detailed balance for the modified moves can be found in Ref. [37]. However, before doing that, we describe the Markov chain steps implemented to modify the gauge field configuration at fixed triangulation, which is a standard extension of the heat-bath algorithms usually adopted in lattice gauge theories.

纯引力 CDT 模拟通常采用局部 Metropolis-Hastings 算法 [33, 34](有趣的是，动力三角化正是实际上需要原始 Metropolis 算法的 Hastings 变体的场景之一: 的确，由于移动会改变随机变量空间，移动及其逆移动的选择概率通常不同，因此其比值会对接受步骤产生影响)，该算法基于一组需要保持三角剖分因果结构的移动——即修改三角剖分时不破坏其叶状结构; 所谓的亚历山大移动 [35, 36] 提供了这样一组合适的移动。在二维情况下，这组移动仅包含三种，通常记为 $(2,2)$, $(2,4)$ 和 $(4,2)$, 用来标记移动前后涉及的单纯形数量。下文我们将简要介绍这些移动，讨论如何修改它们以计入规范构型的对应变化，修改后移动的详细平衡的更详细讨论与证明可参考文献 [37]。但在此之前，我们先介绍固定三角剖分下修改规范场构型的马尔可夫链实现步骤, 这是格点规范理论通常采用的热浴算法的标准推广。

Pure Gauge Move This is similar to what is generally implemented in standard lattice gauge theories and is based on the probability distribution for a given gauge link variable U_l (l is a link of the dual lattice), which stems from Eq. (33) for fixed values of the other gauge link variables:

纯规范移动这与标准格点规范理论中通常实现的操作类似，基于给定规范链接变量 U_l 的概率分布 (l 是对偶格点的一条链接)，该分布由其他规范链接变量固定时的式 (33) 导出:

$$P(U_l)\,dU_l \propto dU_l \exp\left(\frac{\beta}{N}\,\mathrm{Re}\,\mathrm{Tr}\left[U_l F_l^\dagger\right]\right). \tag{35}$$

In Eq. (35), dU_l stands for the gauge-invariant Haar measure over the gauge group, while F_l is the so-called local force acting on that link, $F_l \equiv \sum_{b\ni l}\left(X_b^{(l)}/n_b\right)$ where $X_b^{(l)}$ is the staple going around the bone b , i.e., the ordered product of the other links that form one of the plaquettes containing l (in particular that going around bone b). In general, one can identify two such bones in two dimensions, three in three dimensions, four in four dimensions, and so on; in Fig. 11, we sketch such construction for the two-dimensional case, where the convention chosen for the direction of multiplication of the gauge links around the staple is also clarified. We notice that, once the force F_l has been defined, the probability distribution in Eq. (35) is identical to what is found in standard lattice gauge theories.

式 (35) 中，dU_l 代表规范群上的规范不变哈尔测度，F_l 是作用在该链接上的所谓局部力，$F_l \equiv \sum_{b \ni l} \left(X_b^{(l)} / n_b \right)$ 其中 $X_b^{(l)}$ 是围绕骨 b 的 staple(直积边)，即包含 l 的其中一个面元上其他链接的有序乘积 (具体来说就是围绕骨 b 的那个面元)。一般来说，二维情形可以找到两个这样的骨，三维三个，四维四个，依此类推；图 11 中我们给出了二维情形下该构造的示意图，同时也阐明了 staple 周围规范链接乘法方向的选取约定。可以看到，一旦定义了力 F_l，式 (35) 的概率分布就与标准格点规范理论中的结果完全一致。

The local algorithm then proceeds by selecting randomly a dual link l randomly and by updating the corresponding variable U_l . This can be done by a standard heat-bath algorithm [38,39], i.e., by drawing a new gauge link variable U_l' , in place of U_l , according to the distribution in Eq. (35); the Cabibbo-Marinari algorithm [40] can be also easily implemented for $N > 2$, and microcanonical (over-relaxation) steps can be alternated to improve efficiency.

局部算法的流程是: 随机随机选取一条对偶链接 l，更新对应的变量 U_l。这可以通过标准热浴算法 [38,39] 实现，即按照式 (35) 的分布抽取新的规范链接变量 U_l'，替代 U_l；Cabibbo-Marinari 算法 [40] 也可以很容易地针对 $N > 2$ 实现，还可以交替加入微正则 (过松弛) 步骤来提高效率。

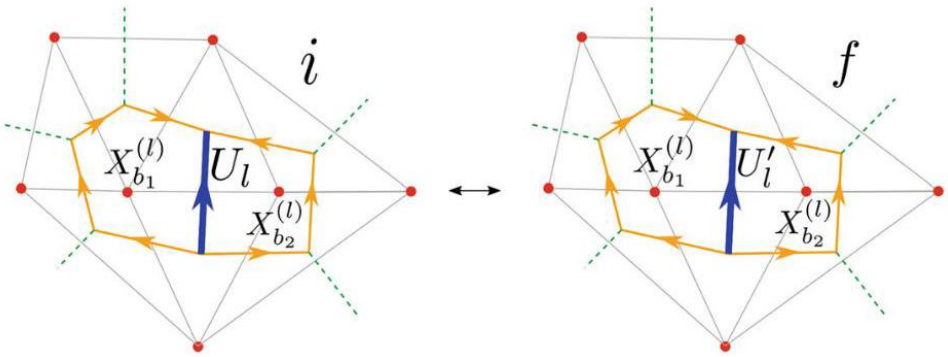

Fig. 11 Sketch of a typical pure gauge move on a two-dimensional causal triangulation, where a single link variable is changed, living on the dual link l (in blue). Here and in the following, the left and right figures indicate, respectively, the initial (i) state and the final (f) one. The orientation of the products of gauge links making up the two staples $X_{b_1}^{(l)}$ and $X_{b_2}^{(l)}$ is indicated by the arrows (orange paths)

图 11 二维因果三角剖分上典型纯规范移动的示意图，图中修改了位于对偶链接 l (蓝色) 上的单个链接变量。下文同理，左右两图分别对应初始 (i) 态和终态 (f)。箭头 (橙色路径) 标出了构成两个 staple $X_{b_1}^{(l)}$ 和 $X_{b_2}^{(l)}$ 的规范链接乘积的方向

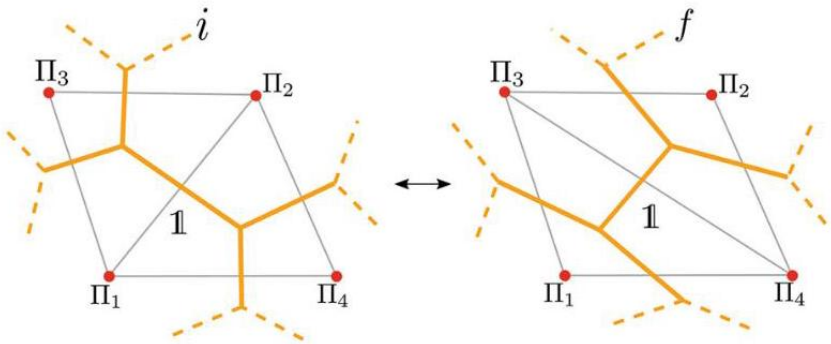

Fig. 12 Sketch of a (2, 2) move. The link dual to the flipped edge is gauge fixed to the identity before the move, so that the four involved plaquettes keep the same value after the move. However, their contribution to the action does changes, because of the modification in the coordination number of the four involved vertices

图 12 (2, 2) 移动的示意图。翻转边对偶的链在移动前被规范固定到单位元，因此涉及的四个面元在移动后保持原有数值。不过它们对作用量的贡献确实会发生变化，因为四个涉及顶点的配位数发生了改变

Triangulation Move (2, 2) This move consists in flipping a time-like edge of the triangulation, hence the link dual to it, as sketched in Fig. 12. The total number of simplices is left unchanged, so the pure-gravity part of the action is untouched; however, the move changes the space $\mathcal{C}_G(\mathcal{T})$ of the gauge configurations. In particular, the coordination number n_1, n_2, n_3 , and n_4 of the four plaquettes appearing in the figure is changed by one unit (plus or minus), and the gauge variable living on the flipped link enters such plaquettes in a different way.

三角剖分移动 (2, 2) 该移动是翻转三角剖分的类时边，即翻转其对偶链，如图 12 所示。单形的总数保持不变，因此作用量的纯引力部分不受影响；但该移动会改变规范构型的空间 $\mathcal{C}_G(\mathcal{T})$ 。具体而言，图中四个面元的配位数 n_1, n_2, n_3 和 n_4 会改变一个单位 (增加或减少)，且翻转链上的规范变量以不同的方式进入这些面元。

An easy way to proceed is to exploit gauge invariance and consider that the Markov move can be viewed as acting from any of the configurations which are gauge equivalent to the starting one, to any of the configurations which are gauge equivalent to the final one, i.e., as a move between two different gauge equivalence classes (orbits). Therefore, by a proper gauge transformation, one can always choose the starting and final configurations such that the gauge variable living on the flipped link is gauge fixed to the identity in both cases: in practice, that means applying a partial gauge fixing before the move is performed. In this way, the four plaquettes involved in the move, $\Pi_{1\leq i\leq 4}$, are left unchanged, even if the gauge action changes anyway, because of the modification in the coordination numbers; however, this is easily taken into account by the Metropolis-Hastings acceptance step.

一种简便的处理方法是利用规范不变性，将马尔可夫移动视为从与初始构型规范等价的任意构型，作用到与最终构型规范等价的任意构型，即视为两个不同规范等价类 (轨道) 之间的移动。因此，通过适当的规范变换，我们总能选取初始和最终构型，使得翻转链上的规范变量在两种情况下都被规范固定为单位元: 实际上这意味着在执行移动前进行部分规范固定。通过这种方式，移动涉及的四个面元 $\Pi_{1\leq i\leq 4}$ 保持不变，尽管规范作用量仍会因配位数的改变而变化；但这一点很容易被梅特罗波利斯-黑斯廷斯接受步处理。

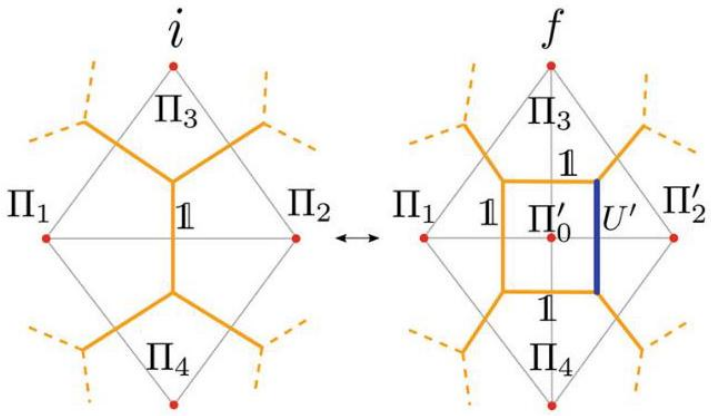

Fig. 13 Sketch of a $(2,4)$ move and of its inverse. Gauge fixing can be used to simplify the move only up to a certain extent. In particular, there is a starting dual link which is transformed into a plaquette of length four: while the starting link can fixed to the identity, the plaquette cannot. After gauge fixing, the link variable U' contains the nontrivial information about the new plaquette

图 13 $(2,4)$ 移动及其逆移动的示意图。规范固定仅能在一定程度上简化移动。具体来说，初始对偶链接会被转变为一个长度为四的面元: 初始链接可以被固定为单位元，但该面元不行。规范固定后，链接变量 U' 包含了新面元的非平凡信息。

Triangulation $(2,4)-(4,2)$ Moves These moves, which are the inverse of each other, are sketched in Fig. 13. They are more involved than the (2, 2) one. They change the volume of the triangulation, creating or eliminating two simplices and a vertex of coordination four, so that the pure-gravity action changes by $\Delta S^{(2,4)}_{CDT} = -\Delta S^{(4,2)}_{CDT} = 2\lambda$, and the gauge configuration is modified substantially, by the introduction or the removal of a central plaquette of length four, which is indicated as Π'_0 in Fig. 13; at the same time, the length and composition of plaquettes $\Pi_{2\leq i\leq 4}$ is changed as well.

三角剖分 $(2,4)-(4,2)$ 移动这些移动互为逆移动，如图 13 所示。它们比 (2,2) 移动更复杂。它们会改变三角剖分的体积，产生或消除两个单形和一个配位数为四的顶点，因此纯引力作用量改变 $\Delta S^{(2,4)}_{CDT} = -\Delta S^{(4,2)}_{CDT} = 2\lambda$ ，同时规范构型发生实质性变化: 引入或移除了一个长度为四的中心面元 (图 13 中标记为 Π'_0)；与此同时，面元 $\Pi_{2\leq i\leq 4}$ 的长度和组成也发生了改变。

The main new difficulty with respect to the $(2,2)$ move is that, since plaquettes are gauge-invariant objects, the appearance of the new plaquette cannot be masked completely by gauge fixing. Indeed, gauge transformations can set to the identity 1 at most three out of four links of the central plaquette Π'_0 , shifting all the physical content in the remaining one. Therefore, during the move, one has to draw at least one new gauge

variable (or destroy it) with a nontrivial distribution, and this must be done properly, i.e., respecting detailed balance.

与 (2, 2) 移动相比，主要的新难点在于: 由于面元是规范不变量，新面元的出现无法被规范固定完全掩盖。实际上，规范变换最多只能将中心面元 Π'_0 的四个链接中的三个设为单位元，将所有物理内容转移到剩下的那个链接上。因此，在移动过程中，必须按照非平凡分布生成 (或消除) 至少一个新的规范变量，且该过程必须处理得当，即满足细致平衡。

Let us consider, for instance, the (2, 4) move. A necessary condition to implement detailed balance is that we can clearly identify pairs of states going into each other under the action of the move and of its inverse. Therefore, while the starting link dual to the two simplices involved in the move can be safely gauge fixed to the identity, the new plaquette, hence the new link U' in Fig. 13, cannot, since in the corresponding inverse (4, 2) move, in which it is destroyed, it will have in general a nontrivial starting value, drawn from the equilibrium distribution of gauge fields in the target triangulation.

我们以 (2, 4) 移动为例。实现细致平衡的必要条件是，我们能够清晰识别出该移动及其逆移动作用下相互转化的状态对。因此，移动涉及的两个单形对应的起始连接可以安全地规范固定为单位元，但新的围道 (即图 13 中的新连接 U') 却不行，因为在对应的、会将它消除的逆 (4, 2) 移动中，它通常拥有非平凡的起始值，该值取自目标三角剖分中规范场的平衡分布。

Therefore, the (2, 4) involves the extraction of a new link variable U' , which then also modifies the value of the plaquette Π'_2 . That can be done in various ways, with the condition that detailed balance be eventually satisfied by the final Metropolis-Hastings acceptance step. However, the most natural choice, which simplifies the final step and improves acceptance, is to draw U' from the heat-bath distribution in the target configuration, i.e., that corresponding to the force $F = \mathbb{1}/4 + X_2/n'_2$. For more details, we refer the reader to Ref. [37].

因此，(2, 4) 过程需要抽取一个新的连接变量 U' ，这也会改变围道 Π'_2 的值。这可以通过多种方式实现，条件是最终的梅特罗波利斯-黑斯廷斯接受步最终满足细致平衡。不过，最自然的选择是从目标构型的热浴分布 (即对应力 $F = \mathbb{1}/4 + X_2/n'_2$ 的分布) 中抽取 U' ，这种选择可以简化最终步骤并提高接受率。更多细节请读者参考文献 [37]。

Perspectives for Higher Dimensions

高维视角

In principle, the approach followed for the two-dimensional case can be extended to higher dimensions. However, the discussion reported above for the (2, 4) and (4, 2) moves clarifies what kind of difficulties may emerge. Let us consider, for example, the analogous (2, 6) and (6, 2) moves for three-dimensional CDT coupled to gauge fields.

原则上，二维情形采用的方法可以推广至高维。不过，上文对 (2,4) 和 (4,2) 移动的讨论已经明确了可能遇到的困难类型。例如，我们来考察耦合规范场的三维 CDT 对应的类似 (2, 6) 和 (6, 2) 移动。

In this case, two adjacent tetrahedra sharing a triangle are transformed into six tetrahedra, or vice versa, by splitting the common triangle into three triangles. From the point of view of the dual graph, the link connecting the starting tetrahedra gets transformed into a triangular prism, made up 9 link variables and 5 new plaquettes, two of length 3 and three of length 4 . The information contained in this new geometrical structure can be only partially reduced by gauge fixing. In particular, gauge fixing along a maximal three can fix to the identity only 5 of the 9 links of the prism (see Fig. 14). That means that, in order to perform the move, one has to draw 4 new link variables at the same time, and take into account, for the final acceptance step, the modification of more than 10 plaquettes.

这种情况下，共享一个三角形的两个相邻四面体可以通过将公共三角形拆分为三个三角形，变换为六个四面体，反之亦然。从对偶图的角度来看，连接初始两个四面体的链接会变换为一个三棱柱，包含 9 个链接变量和 5 个新格团，其中 2 个长度为 3，3 个长度为 4。这种新几何结构包含的信息仅能通过规范固定部分约化。具体来说，沿最大树进行规范固定仅能将三棱柱 9 个链接中的 5 个固定为恒等元 (见图 14)。这意味着，为了执行该移动，必须同时生成 4 个新链接变量，并且在最终接受步骤中需要考虑超过 10 个格团的变化。

The above reasoning can be easily generalized to the case of generic space-time dimension D for the analogous $(2, 2D)$ move and its inverse. The number of new gauge links to be created after the direct move is $2D + 2D\,(D-1)\,/2 = D^2$; the number of involved dual lattice sites usable for gauge fixing is $2D$; however, they lie on a closed hypersurface, so the number of gauge links which can be actually gauge fixed to the identity is $2D-1$. Finally, one is left with $(D-1)^2$ new link variables to be drawn at the same time.

上述推理可以很容易推广到任意时空维度 D 中类似的 $(2, 2D)$ 移动及其逆移动的情况。正向移动后需要生成的新规范链接数为 $2D + 2D\,(D-1)\,/2 = D^2$ ；可用于规范固定的相关对偶格点数目为 $2D$ ；但这些格点位于封闭超曲面上，因此实际可规范固定为单位元的规范链接数为 $2D-1$ 。最终，我们需要同时抽取 $(D-1)^2$ 个新的链接变量。

This simple counting illustrates the technical difficulties emerging in higher dimensions, also related to the need for having a reasonable acceptance rate. As a consequence, while work is still in progress along this direction, an extension of the algorithms developed in Ref. [37] to 3D and 4D CDT has not been finalized yet (Fig. 14).

这种简单计数说明了高维下出现的技术难题，这些难题也与对合理接受率的需求相关。因此，尽管目前该方向的研究仍在进行中，文献 [37] 中开发的算法尚未完成向三维和四维 CDT 的推广 (图 14)。

Fig. 14 Sketch of a possible implementation of the $(2, 6)$ and $(6, 2)$ moves on a three-dimensional causal triangulation, where four dynamical link variables (in blue) remain dynamical after gauge fixing; orange links show links gauge fixed to identity

图 14 三维因果三角剖分中 $(2, 6)$ 和 $(6, 2)$ 移动一种可能实现的示意图，其中四个动力学链接变量 (蓝色) 在规范固定后仍保持动力学；橙色链接表示已被规范固定为恒等元的链接

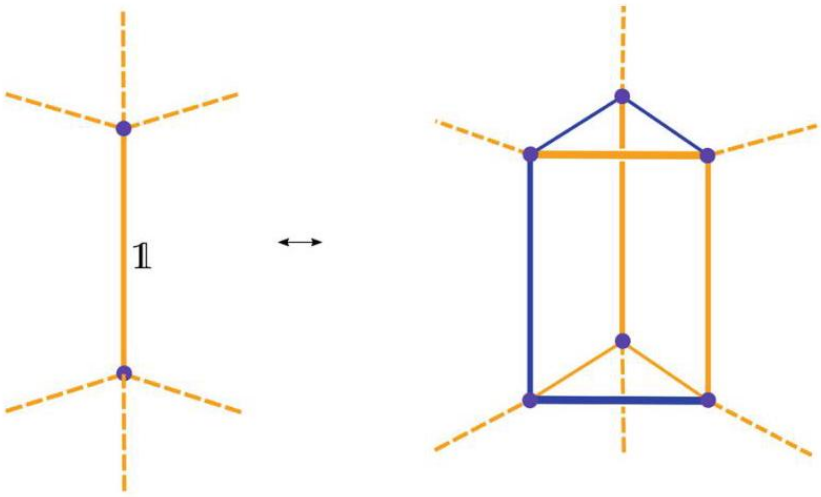

Gauge Fields on Dynamical Triangulations at Work

作用于动态三角剖分上的规范场

In this section, we discuss some numerical results from simulations of 2D CDT coupled to Yang-Mills theories, considering both the $U(1)$ and $SU(2)$ gauge group. A detailed account of such results can be found in Ref. [37]. Here, we only focus on a few aspects, which could be of particular interest when algorithms for higher dimensions will be available.

在本节中，我们讨论耦合杨-米尔斯理论的二维因果动态三角剖分 (CDT) 模拟得到的若干数值结果，同时考虑了 $U(1)$ 规范群和 $SU(2)$ 规范群。这类结果的详细说明可见文献 [37]。本文仅关注少数几个方面，当适用于更高维度的算法开发完成后，这些方面会具有特殊的研究价值。

The first aspect regards how the critical behavior of the pure-gravity theory is modified by the presence of gauge fields. This is of course relevant to the search for a critical point where a renormalized theory of quantum gravity could eventually be defined, since the coupling to other fields, either matter or gauge, modifies the renormalization group flow. As we will discuss, the two-dimensional case is somewhat trivial in this respect, since the coupling to gauge fields just renormalizes the cosmological constant and shifts its critical value, leaving critical indices unchanged.

第一个方面是规范场的存在如何改变纯引力理论的临界行为。这对于寻找可最终定义重整化量子引力理论的临界点至关重要，因为与其他场 (物质场或规范场) 的耦合会改变重整化群流。我们将会谈到，二维情况在这方面相对平凡，因为与规范场的耦合仅会重整宇宙学常数、偏移其临界值，不会改变临界指数。

As a second aspect, we consider the definition and behavior of gauge observables in the fluctuating spacetime geometry. Among various possible gauge-invariant quantities (see Ref. [37] for a more detailed discussion), we focus our attention here on observables related to the topology of gauge fields, in particular on the so-called winding number (or topological charge): this quantity classifies the possible mappings of the gauge

group onto the space-time manifold; therefore, it could be particularly interesting in a situation in which the latter is not fixed but instead fluctuating.

第二个方面，我们研究涨落时空几何中规范可观测量的定义与行为。在各类可能的规范不变量中(更详细的讨论见文献 [37])，本文重点关注与规范场拓扑相关的可观测量，即所谓的绕数 (或称拓扑荷): 该量对规范群到时空流形的所有可能映射进行分类；因此，在时空流形不固定、本身存在涨落的场景下，它会具有特殊的研究意义。

Before starting the discussion of results, let us briefly recap the main features of our simulations. The parameters entering the discretized theory are the bare cosmological constant λ , see Eq. (34), and the inverse gauge coupling $\beta \propto 1/g^2$, see Eq. (33), which differs from standard definitions used in lattice gauge theories by a proportionality factor, related to the bone coordination numbers n_b and to the fact that the reference flat discretization is hexagonal, rather than square, lattice. A further parameter is the number of temporal slices N_t , which is fixed, while the spatial extension of each slice is dynamical. The overall imposed topology is that of a torus, with periodic boundary conditions in the temporal and spatial directions: because of the Gauss-Bonnet theorem in two dimensions, which implies a globally flat geometry, i.e., the condition $\langle n_b \rangle = 6$ holds for all sampled triangulations.

在开始讨论结果之前，我们先简要回顾我们模拟的核心特征。离散化理论涉及的参数包括裸宇宙学常数 λ (见式 (34))，以及逆规范耦合 $\beta \propto 1/g^2$ (见式 (33))，该逆规范耦合与格点规范理论中使用的标准定义不同，相差一个与骨配位数 n_b 相关的比例因子，此外还因为参考平直离散化是六角格而非正方形格点。另一个参数是固定的时间切片数 N_t ，每个切片的空间延展是动力学的。我们设定的整体拓扑为环面，时间方向和空间方向都采用周期性边界条件: 这是因为二维情况下的高斯-博内定理要求整体平直几何，即所有采样三角剖分都满足条件 $\langle n_b \rangle = 6$ 。

Critical Behavior

临界行为

The pure-gravity theory undergoes a continuous transition for a critical cosmological parameter $\lambda_c = \log(2)$. As the critical point is approached from above, one observes a divergence both of the average total volume $\langle V \rangle$ of the triangulation and of the length $\xi_{\text{Vprof.}}$ describing the large distance behavior of the correlation between the spatial extensions of pairs of different time slices, i.e., the two-point function of the so-called volume profile. The critical behavior is described in terms of two critical indices υ and μ :

纯引力理论在临界宇宙学参数 $\lambda_c = \log(2)$ 处发生连续相变。当从临界点上方趋近该点时，可观测到三角剖分的平均总体积 $\langle V \rangle$ ，以及描述不同时间切片空间延展对关联大尺度行为 (即所谓体积轮廓两点关联函数) 的关联长度 $\xi_{\text{Vprof.}}$ 均发散。临界行为由两个临界指数 υ 和 μ 描述:

$$\langle V \rangle \propto (\lambda - \lambda_c)^{-\mu}, \ \xi_{\text{Vprof.}} \propto (\lambda - \lambda_c)^{-\nu}. \tag{36}$$

Such scaling laws are expected to hold sufficiently close to λ_c , i.e., in the so-called scaling window; results of Ref. [37] show that the scaling window for $\xi_{\text{Vprof.}}$ is somewhat larger than that for $\langle V \rangle$.

这类标度律在足够靠近 λ_c 的区域，即所谓标度窗口内成立；文献 [37] 的结果表明，$\xi_{\text{Vprof.}}$ 的标度窗口略大于 $\langle V \rangle$ 的标度窗口。

The addition of gauge fields is not expected to lead to a significant modification of the critical behavior. Indeed, it is known that two-dimensional gauge fields can be easily integrated away [41-43]. Nevertheless, on a curved geometry, one is left with a nontrivial contribution, depending on the coordination numbers n_b , which could modify the behavior of gravity observables.

引入规范场不会显著改变临界行为，因为众所周知二维规范场可直接积分消去 [41-43]。但在弯曲几何上，会留下依赖配位数 n_b 的非平凡贡献，这可能改变引力观测量的行为。

In Fig. 15, we report the behavior of the correlation length as a function of λ for $\beta = 1$ and the $U(1)$ gauge group: results can still be nicely fitted according the scaling ansatz of Eq. (36), however with a different λ_c compared to the pure gravity case. The critical values of λ obtained for $U(1)$ and $SU(2)$ are reported in the same figure as a function of β , together with an analytical prediction based on a strong coupling expansion of the gauge theory, i.e., a series expansion in β [37].

图 15 给出了关联长度随 λ 变化的行为，对应 $\beta = 1$ 和 $U(1)$ 规范群: 结果仍可通过式 (36) 的标度假设很好拟合，但临界指数 λ_c 与纯引力情形不同。图中同时给出了 $U(1)$ 和 $SU(2)$ 对应的 λ 临界值随 β 的变化，以及基于规范场强耦合展开 (即 β 的级数展开) 得到的解析预言 [37]。

Despite the change in the critical coupling, no appreciable change is observed, within errors, for the critical indices, as can be appreciated from Fig. 16, where the values of υ obtained for different β and gauge groups are reported. To confirm the apparent stability of υ , we have performed a global fit of all values to a constant, obtaining $\upsilon = 0.496\,(7)\left(\chi^2/\text{ dof } = 9.1/9\right)$. We notice that this value is compatible with a mean field critical index 1/2 .

如图 16 所示 (图中给出了不同 β 和不同规范群对应的 υ 取值)，在误差范围内，除临界耦合发生改变外，并未观测到临界指数的明显变化。为了证实 υ 的表观稳定性，我们对所有取值做了全局常数拟合，得到 $\upsilon = 0.496\,(7)\left(\chi^2/\text{ dof } = 9.1/9\right)$。我们注意到该取值与平均场临界指数 1/2 相容。

These observations suggest that, in the two-dimensional case, the presence of gauge fields modifies gravity just by an additive renormalization of the cosmological constant. The fact that local fluctuations of n_b are not relevant could be explained by the seemingly mean field behavior. Of course, the situation could be quite different in higher dimensions.

这些观测结果表明，在二维情形下，规范场的存在仅通过对宇宙常数的可加重整化改变引力。n_b 的局域涨落不相关这一点，可以用表观平均场行为解释。当然，在更高维度情况可能大不相同。

As a final comment, it is clear that approaching λ_c at fixed inverse gauge coupling β is not enough to define a proper continuum limit for the whole theory. One should tune also β so that gauge-related correlation lengths diverge at the same time: in two space-time dimensions, this is usually achieved as $\beta \to \infty$, with an asymptotic scaling of gauge correlation lengths proportional to $\sqrt{\beta}$.

最后需要说明，在固定规范反耦合 β 下趋近 λ_c ，不足以定义整个理论合适的连续极限。还需要调整 β ，使得和规范场相关的关联长度同时发散: 在二维时空下，这通常在 $\beta \to \infty$ 时实现，此时规范关联长度的渐近标度正比于 $\sqrt{\beta}$ 。

Gauge Topology

规范拓扑

In two space-time dimensions, a topological classification of gauge configurations applies only to the case of $U(1)$ gauge group. In this case, the topological charge Q , or winding number, amounts to the total flux of the gauge field strength across the space-time manifold: gauge configurations with a non-integer topological charge are completely suppressed from the path integral if the manifold is compact (like in our case, since we are on a torus) or if vanishing conditions at infinity are imposed on the field strength, so that relevant contributions to the path integral can be classified according to integer values of Q .

在二维时空下，规范构型的拓扑分类仅适用于 $U(1)$ 规范群的情况。这种情况下，拓扑荷 Q (即绕数) 等于规范场强度在整个时空流形上的总通量: 如果流形是紧致的 (就像我们的情况，我们研究的是环面)，或者场强度满足无穷远零边界条件，那么路径积分中会完全排除非整数拓扑荷的规范构型，因此路径积分的相关贡献可以按照 Q 的整数值分类。

The very concept of homotopy classes is lost on a discrete space-time but is recovered as the continuum limit is approached. A side effect of that, however, is the fact that, as the inverse gauge coupling β grows, standard updating algorithms become extremely inefficient in moving from one topological sector to the other, so that ergodicity is lost: this problem is usually known as topological freezing and affects standard simulations of lattice gauge theories [44-47].

在离散时空中原同伦类的概念不再成立，但当趋近连续极限时可以重新得到。不过由此带来的一个副作用是，随着反规范耦合 β 增大，标准更新算法在不同拓扑扇区之间切换的效率会变得极低，从而导致遍历性丧失: 这个问题通常被称为拓扑冻结，是格点规范理论标准模拟中存在的已知问题 [44-47]。

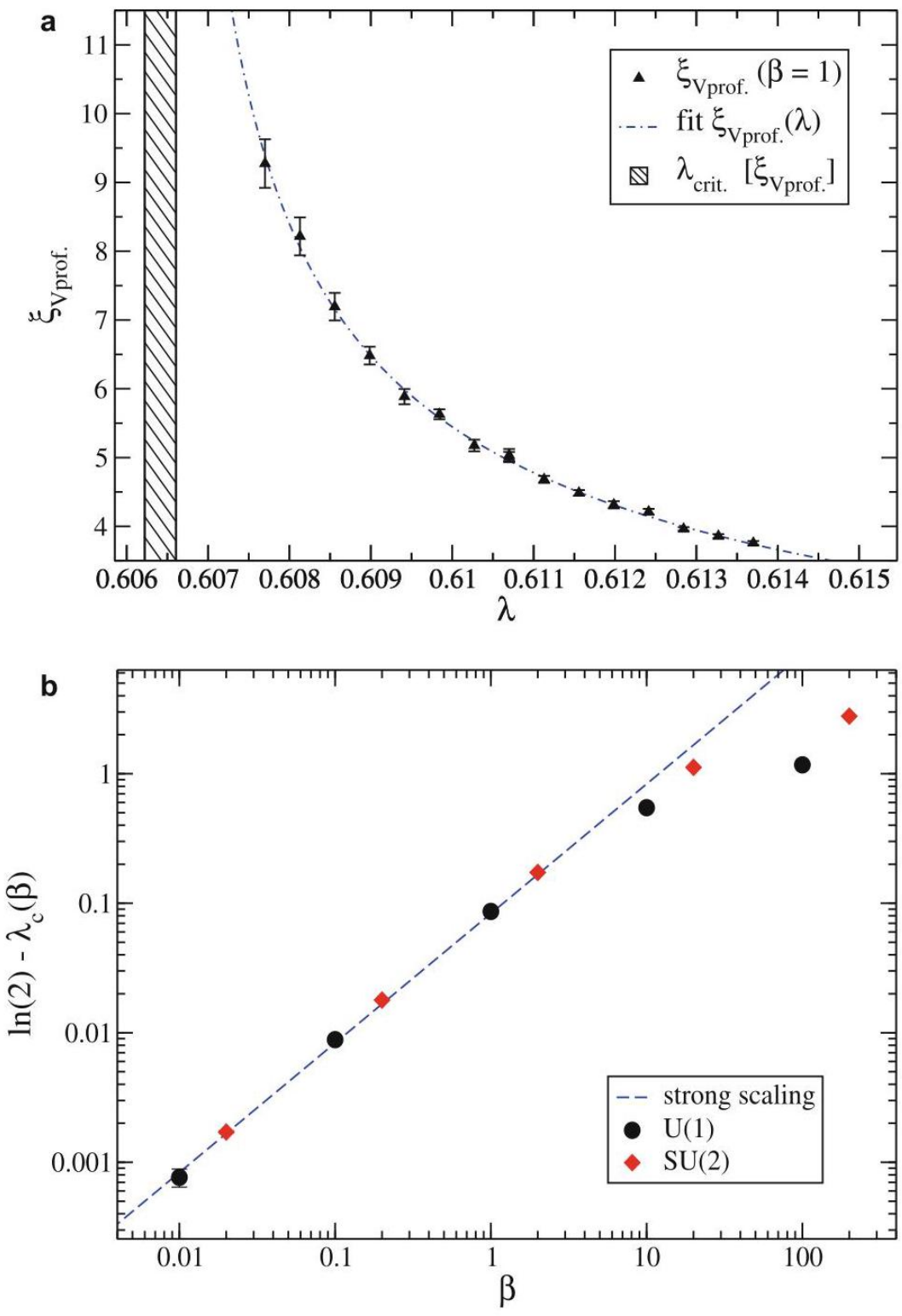

Fig. 15 Left: determination of $\xi_{\text{Vprof.}}$ as a function of λ for the $U(1)$ gauge group at $\beta = 1$, together with the results of a fit to a power law behavior as in Eq. (36). Right: critical values of λ for $U(1)$ and $SU(2)$ as a function of β; the dashed line represents the strong coupling expansion prediction discussed in the text

图 15 左: $U(1)$ 规范群在 $\beta = 1$ 下，$\xi_{\text{Vprof.}}$ 随 λ 变化的测定结果，同时给出了对式 (36) 幂律行为的拟合结果。右: $U(1)$ 和 $SU(2)$ 的 λ 临界值随 β 的变化；虚线表示本文讨论的强耦合展开预测

Within our formulation, it is relatively easy to define an integer-valued topological charge even on the discretized manifold:

在我们的表述框架下，即使在离散化流形上也能相对容易地定义整数值拓扑荷:

$$Q \equiv \frac{1}{2\pi} \sum_{b \in \mathcal{T}^{(d-2)}} \arg\left[\mathrm{Tr}\left(\Pi_b\right)\right] \tag{37}$$

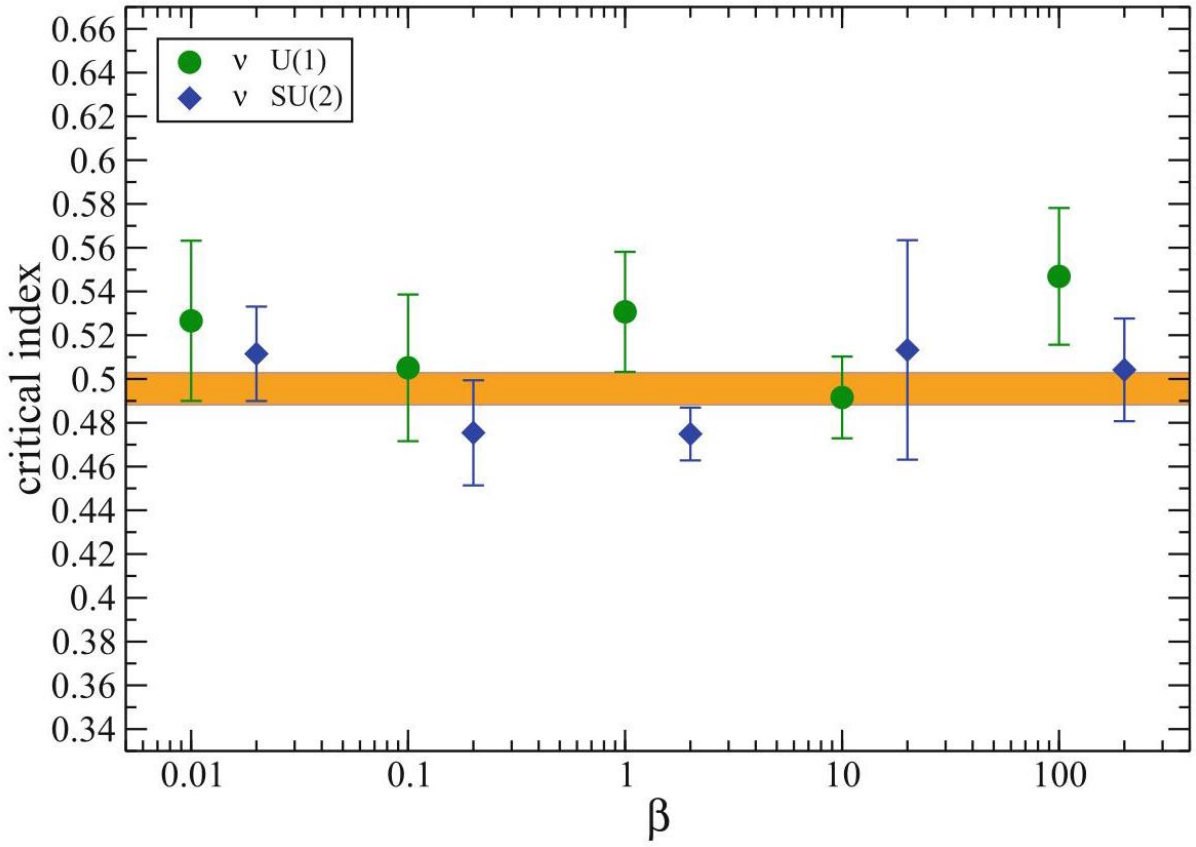

Fig. 16 Critical index υ , as a function of the bare gauge coupling β , for both explored gauge groups. The horizontal bands are the result of a best fit to constant value

图 16 两种已研究规范群的临界指标 υ 随裸规范耦合 β 的变化。水平带是对常数值的最佳拟合结果

where Π_b is the plaquette around vertex b , and the argument function arg z returns values in $(-\pi, \pi]$.

其中 Π_b 是顶点 b 周围的基元面片，辐角函数 arg z 返回 $(-\pi, \pi]$ 范围内的值。

In the following, we discuss briefly results obtained for Q and for the so-called topological susceptibility $\chi \equiv \langle Q^2 \rangle / V$, comparing results from numerical simulations on a triangulation with fixed geometry, corresponding in particular to a flat torus, with those from dynamical simulations in which the geometry is updated

as well. To start with, in Fig. 17, we compare the Monte Carlo histories of Q obtained in the two cases for $\beta = 60$ and $\beta = 70$. In order to make the comparison meaningful, we tuned λ so has to have an average volume $\langle V \rangle$ equal to the volume used for the fixed geometry case.

在下文中，我们简要讨论针对 Q 和所谓拓扑磁化率 $\chi \equiv \langle Q^2 \rangle / V$ 得到的结果，比较了固定几何三角剖分 (特别是平直环面情况) 的数值模拟结果，与同时更新几何的动力学模拟结果。首先，在图 17 中，我们比较了两种情况下 $\beta = 60$ 和 $\beta = 70$ 对应的 Q 蒙特卡罗历史。为了使比较有意义，我们调整 λ，使得平均体积 $\langle V \rangle$ 等于固定几何情况所用的体积。

Topological freezing emerges quite clearly in static simulations; indeed, Q is fully frozen at $\beta = 70$; the interesting result is that, on the contrary, no freezing at all is observed in the dynamical case. We have checked that this phenomenon is induced by the typical roughness of the triangulation, rather than by its dynamical change during the Monte Carlo evolution (see Ref. [37] for details). A possible explanation of this substantial improvement in the decorrelation of Q could be searched in the existence of regions with a large negative curvature (i.e., of vertices with a large coordination number n_b), where large fluctuations in the local flux of the field strength across the manifold are possible, with a limited expense in terms of the pure gauge action. It is reasonable to guess that this feature could extend to the higher-dimensional case as well.

拓扑冻结在静态模拟中表现得非常明显；实际上 Q 在 $\beta = 70$ 处完全冻结；而有意思的结果是，动力学情况中完全没有观测到冻结现象。我们验证了，这种现象是由三角剖分的本征粗糙度导致的，而非蒙特卡罗演化过程中的动力学变化 (细节见文献 [37])。对于 Q 去关联能力的大幅提升，一种可能的解释是，流形中存在大负曲率区域 (即配位数目很大的顶点 n_b)，在这些区域，即使纯规范作用的代价很低，也能发生场强度局域通量的大幅涨落。我们有理由推测，这一特性也可以推广到更高维的情况。

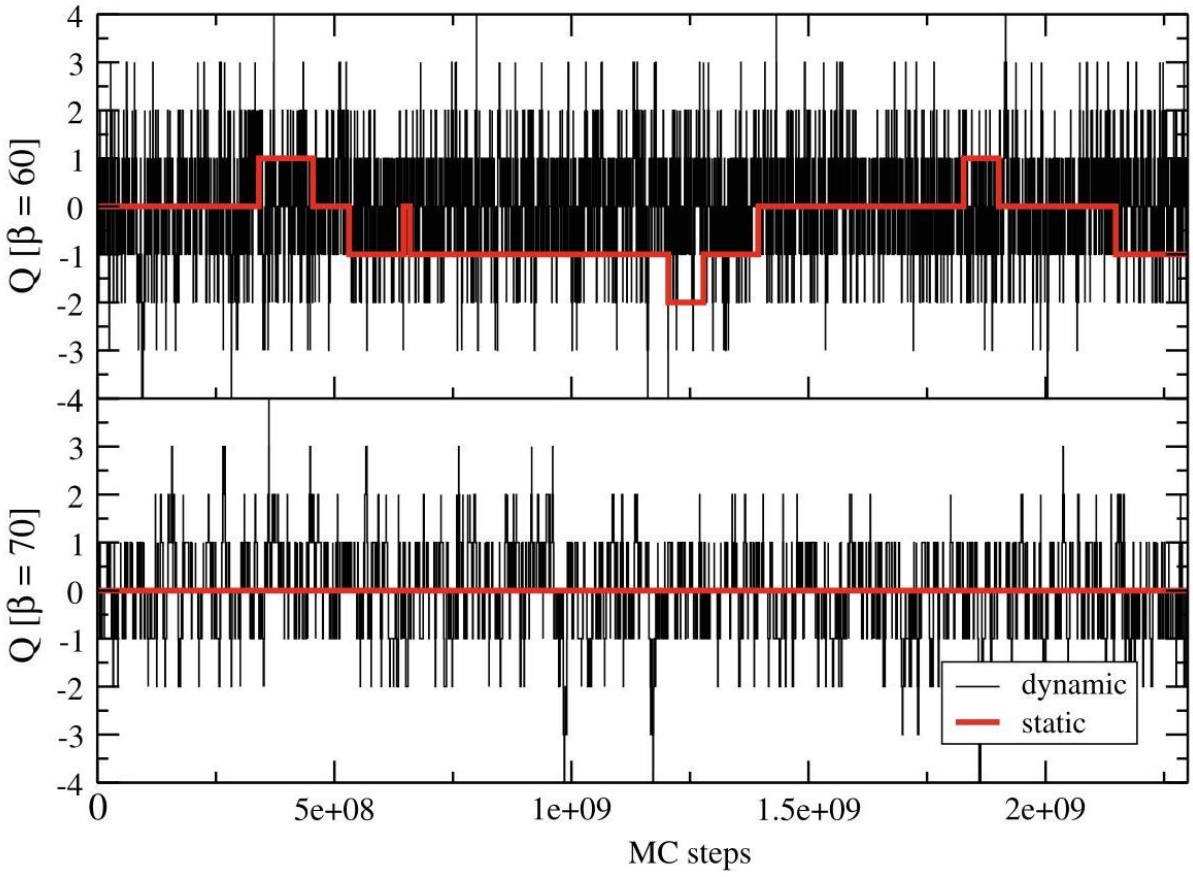

Fig. 17 Comparison of the Monte Carlo histories of Q for the dynamic and static (flat) simulations with a comparable total volume $\langle V \rangle = 800$ and for two different inverse gauge couplings, $\beta = 60$ and $\beta = 70$

图 17 总体积 $\langle V \rangle = 800$ 相近时，动力学和静态 (平直) 模拟在两种不同反规范耦合 $\beta = 60$ 和 $\beta = 70$ 下的 Q 蒙特卡罗历史对比

To conclude, in Fig. 18, we show results obtained for the topological susceptibility (times β), comparing again the flat static and the dynamical case. We stress that, in the dynamical case, an ambiguity emerges in the definition of χ , since the total volume itself fluctuates; our prescription is to define $\chi_Q \equiv \left\langle \frac{Q^2}{V} \right\rangle$, i.e., volume fluctuations are taken into account and included in one single average. Slight differences are observed at finite β , however, the improved decorrelation of Q in the dynamical case allows to obtain accurate results even at large values of β . Assuming $1/\beta$ corrections and considering only data with $\beta > 30$, we have tried to extract a continuum extrapolation (however, at fixed gravity coupling) obtaining $\beta\chi_Q = 0.0758\,(14)$ with a reduced chi-squared $\chi^2/\,\mathrm{dof} = 1.6/3$: such result is in good agreement with the prediction for the flat continuum theory [43], $\beta\chi_Q = 3/\left(4\pi^2\right) \simeq 0.075991$, where we have taken into account an additional factor 6 in our definition of β .

总而言之，在图 18 中，我们展示了拓扑磁化率 (乘以 β) 的结果，再次对比了平坦静态情形与动力学情形。我们强调，在动力学情形中，χ 的定义存在歧义，因为总体积本身是涨落的；我们的规则是定义 $\chi_Q \equiv \left\langle \frac{Q^2}{V} \right\rangle$，即体积涨落已被考量并纳入单次平均当中。在有限 β 下观测到了微小差异，但动力学情形中 Q 的退相关性更优，因此即使在 β 取大值时也能得到精确结果。假设存在 $1/\beta$ 修正且仅考虑满足 $\beta > 30$ 的数据，我们尝试提取连续极限外推 (但固定引力耦合)，得到 $\beta\chi_Q = 0.0758\,(14)$，约化卡方为 $\chi^2/$，自由度为 $= 1.6/3$：该结果与平坦连续理论的预测 [43] 吻合良好，即 $\beta\chi_Q = 3/\left(4\pi^2\right) \simeq 0.075991$，我们在 β 的定义中已经考虑了额外的因子 6。

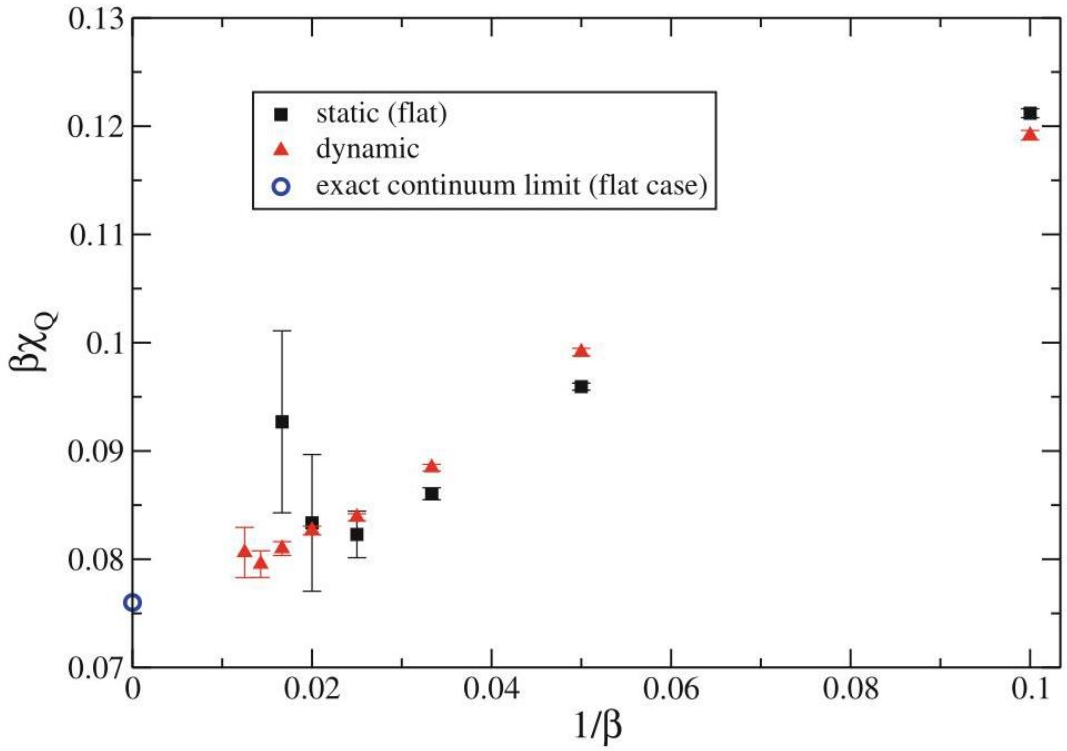

Fig. 18 Comparison of the topological susceptibilities $\langle Q^2/V \rangle$ obtained for the static (flat) and dynamic simulations at average volume $V = 800$

图 18 平均体积 $V = 800$ 下，静态 (平坦) 模拟与动力学模拟得到的拓扑磁化率 $\langle Q^2/V \rangle$ 对比

Summary

摘要

This chapter has been devoted to a few recent developments regarding the CDT approach to quantum gravity. As a first topic, in section "Spectral Methods", we have discussed the need for new physical quantities characterizing the CDT phase diagram, focusing on spectral observables. We showed how information about the effective dimension at large scales and the characteristic scales of ensembles of geometries can be extracted from the spectrum and discussed another possible discretization. However, there is still much to be investigated in the form of analysis of the properties of eigenvectors, such as their localization properties or a

coarse-graining procedure for local observables by spectral projection in the eigenspace corresponding to the lowest part of the spectrum.

本章致力于介绍量子引力因果动态三角剖分 (CDT) 方法的若干最新进展。作为第一个主题，我们在「谱方法」一节讨论了表征 CDT 相图需要引入新物理量，并聚焦于谱可观测量。我们展示了如何从谱中提取大尺度有效维度以及几何系综特征尺度的信息，还讨论了另一种可能的离散化方案。然而，仍有诸多内容有待研究，例如本征向量性质分析，包括本征向量的局域化性质，或是对谱低端对应本征空间通过谱投影构造局域可观测量粗粒化流程。

As a second topic, we have discussed how the CDT approach could be enlarged to include a minimal coupling to Abelian and non-Abelian gauge fields. While the general formulation is clear, present algorithms limit the exploration to the two-dimensional case. As a preliminary step, which is possible already with available algorithms, one could perform numerical simulations of gauge theories on fixed triangulations sampled via pure-gravity CDT simulations: that would not give any information on the feedback of gauge fields on gravity, however, could reveal interesting aspects about the influence of the underlying space-time geometry on gauge field dynamics.

作为第二个主题，我们讨论了如何扩展 CDT 方法，使其包含阿贝尔与非阿贝尔规范场的最小耦合。尽管整体框架已经清晰，现有算法仅能支持探索二维情形。利用现有算法已经可以开展一个初步工作: 对纯引力 CDT 模拟抽取的固定三角剖分进行规范场论数值模拟，虽然这无法得到规范场对引力的反馈信息，但可以揭示底层时空几何对规范场动力学的影响这一有趣内容。

Acknowledgments GC acknowledges support from the National Centre on HPC, Big Data and Quantum Computing - SPOKE 10 (Quantum Computing) and received funding from the European Union Next-GenerationEU - National Recovery and Resilience Plan (NRRP) - MISSION 4 COMPONENT 2, INVESTMENT N. 1.4 - CUP N. I53C22000690001.

致谢 GC 感谢国家高性能计算、大数据与量子计算中心——SPOKE 10(量子计算) 的支持，本研究得到欧盟下一代欧盟计划、意大利国家复苏与韧性计划 (NRRP)——任务 4 第 2 部分，第 1.4 项投资资助，项目编号 CUP N. I53C22000690001。

References

参考文献

1. M. Reuter, F. Wolter, M. Shenton, M. Niethammer, Laplace-Beltrami eigenvalues and topological features of eigenfunctions for statistical shape analysis. Comput. Aided Des. 41(10), 739 (2009)

2. M. Reuter, F. Wolter, M. Shenton, M. Niethammer, Comput. Aided Des. 38(4), 342 (2006)

3. M. Belkin, P. Niyogi, Laplacian eigenmaps and spectral techniques for embedding and clustering, in Proceedings of NIPS'01 (2001), pp. 585-591

4. D.V. Vassilevich, Heat kernel expansion: user's manual. Phys. Rept. 388, 5 (2003)

5. P.W. Anderson, Absence of diffusion in certain random lattices. Phys. Rev. 109, 1492-1505 (1958)

6. L. Ujfalusi, M. Giordano, F. Pittler, T.G. Kovacs, I. Varga, Anderson transition and multifractals in the spectrum of the Dirac operator of Quantum Chromodynamics at high temperature. Phys. Rev. D 92(9), 094513 (2015). [arXiv:1507.02162 [cond-mat.dis-nn]]

7. D. ben-Avraham, S. Havlin, Diffusion and Reactions in Fractals and Disordered Systems (Cambridge University, Cambridge, 2005)

8. J. Ambjørn, D. Boulatov, J.L. Nielsen, J. Rolf, Y. Watabiki, The spectral dimension of 2-D quantum gravity. JHEP 02, 010 (1998). arXiv:hep-th/9801099

9. J. Ambjørn, J. Jurkiewicz, R. Loll, The spectral dimension of the universe is scale dependent. Phys. Rev. Lett. 95, 171301 (2005). arXiv:hep-th/0505113

10. J. Ambjorn, J. Jurkiewicz, R. Loll, Reconstructing the universe. Phys. Rev. D 72, 064014 (2005)

11. H.P. McKean, I. Singer, Curvature and the eigenvalues of the Laplacian. J. Differ. Geom. 1(1), 43 (1967)

12. H. Weyl, Nachr. Königl. Ges. Wiss. Göttingen, 110-117 (1911).

13. V. Ivrii, 100 years of Weyl's law. Bull. Math. Sci. 6(3), 379-452 (2016). [arXiv:1608.03963v2 [math.SP]]

14. G. Clemente, M. D'Elia, Spectrum of the Laplace-Beltrami operator and the phase structure of causal dynamical triangulations. Phys. Rev. D 97, 124022 (2018). [arXiv:1804.02294 [hep-th]]

15. J. Cheeger, A lower bound for the smallest eigenvalue of the Laplacian, in Problems in Analysis (Symposium in honor of Salomon Bochner, Princeton University, Princeton, N.J., 1969). (Princeton University Press, Princeton, N.J., 1970), pp. 195-199

16. J. Ambjorn, S. Jordan, J. Jurkiewicz, R. Loll, A Second-order phase transition in CDT. Phys. Rev. Lett. 107, 211303 (2011). [arXiv:1108.3932 [hep-th]]

17. J. Ambjorn, S. Jordan, J. Jurkiewicz, R. Loll, Second- and first-order phase transitions in CDT. Phys. Rev. D 85, 124044 (2012). [arXiv:1205.1229 [hep-th]]

18. J. Ambjørn, J. Gizbert-Studnicki, A. Görlich, J. Jurkiewicz, N. Klitgaard, R. Loll, Characteristics of the new phase in CDT. Eur. Phys. J. C 77, 152 (2017). [arXiv:1610.05245 [hep-th]]

19. J. Ambjorn, D. Coumbe, J. Gizbert-Studnicki, A. Gorlich, J. Jurkiewicz, New higher-order transition in causal dynamical triangulations. Phys. Rev. D 95, 124029 (2017). [arXiv:1704.04373 [hep-lat]]

20. J. Ambjorn, J. Jurkiewicz, R. Loll, Phys. Rev. Lett. 93, 131301 (2004). [hep-th/0404156]

21. M. Reitz, D. Németh, D. Rajbhandari, A. Görlich, J. Gizbert-Studnicki, Generalised spectral dimensions in non-perturbative quantum gravity. Classical Quantum Gravity 40(12), 125003. [arXiv:2207.05117 [gr-qc]]

22. F. Caceffo, G. Clemente, Spectral analysis of causal dynamical triangulations via finite element method. Phys. Rev. D 107(7), 074501 (2023). [arXiv:2010.07179 [hep-lat]]

23. G. Allaire, A. Craig, Numerical Analysis and Optimization (Oxford University, Oxford, 2007)

24. T.J.R. Hughes, The Finite Element Method: Linear Static and Dynamic Finite Element Analysis (Dover Publications, New York, 2000)

25. G. Strang, G. Fix, An Analysis of the Finite Element Method (Wellesley-Cambridge Press, Wellesley, 2008)

26. O.C. Zienkiewicz, R.L. Taylor, J.Z. Zhu, The Finite Element Method: Its Basis and Fundamentals (Butterworth-Heinemann, Oxford, 2013)

27. B. Szabó, I. Babuska, Finite Element Analysis (Wiley-Interscience, New York, 1991)

28. G. Clemente, M. D'Elia, A. Ferraro, Running scales in causal dynamical triangulations. Phys. Rev. D 99(11), 114506 (2019). [arXiv:1903.00430 [hep-th]]

29. G. Clemente, M. D'Elia, A. Ferraro, Spectral Methods in Causal Dynamical Triangulations. PoS Lattice2019, p. 116. arXiv:1912.11311 [hep-lat]

30. K.G. Wilson, Confinement of Quarks. Phys. Rev. D 10, 2445-2459 (1974)

31. T. Regge, General relativity without coordinates. Nuovo Cim. 19, 558 (1961)

32. J. Ambjorn, A. Goerlich, J. Jurkiewicz, R. Loll, Nonperturbative quantum gravity. Phys. Rept. 519, 127 (2012). [arXiv:1203.3591 [hep-th]]

33. N. Metropolis, A.W. Rosenbluth, M.N. Rosenbluth, A.H. Teller, E. Teller, Equation of state calculations by fast computing machines. J. Chem. Phys. 21, 1087 (1953)

34. W.K. Hastings, Monte Carlo sampling methods using Markov chains and their applications. Biometrika 57, 97 (1970)

35. J.W. Alexander, The combinatorial theory of complexes. Ann. Mat. 31, 292 (1931)

36. J. Ambjørn, J. Jurkiewicz, R. Loll, Lorentzian and Euclidean quantum gravity—analytical and numerical results. NATO Sci. Ser. C 556, 381 (2000). [arXiv:hep-th/0001124 [hep-th]]

37. A. Candido, G. Clemente, M. D'Elia, F. Rottoli, Compact gauge fields on Causal Dynamical Triangulations: a 2D case study. JHEP 04, 184 (2021). [arXiv:2010.15714 [hep-lat]]

38. M. Creutz, Monte Carlo study of quantized SU(2) gauge theory. Phys. Rev. D 21, 2308 (1980)

39. A.D. Kennedy, B.J. Pendleton, Improved heat bath method for Monte Carlo calculations in lattice gauge theories. Phys. Lett. B 156, 393 (1985)

40. N. Cabibbo, E. Marinari, A new method for updating SU(N) matrices in computer simulations of gauge theories. Phys. Lett. B 119, 387-390 (1982). doi:10.1016/0370-2693(82)90696-7

41. J. Ambjorn, A. Ipsen, Two-dimensional causal dynamical triangulations with gauge fields. Phys. Rev. D 88(6), 067502 (2013). [arXiv:1305.3148 [hep-th]]

42. C. Cao, M. van Caspel, A.R. Zhitnitsky, Topological Casimir effect in Maxwell electrodynamics on a compact manifold. Phys. Rev. D 87, 105012 (2013). [arXiv:1301.1706 [hep-th]]

43. C. Bonati, P. Rossi, Topological susceptibility of two-dimensional $U(N)$ gauge theories. Phys. Rev. D 99, 054503 (2019). [arXiv:1901.09830 [hep-lat]]

44. B. Alles, G. Boyd, M. D'Elia, A. Di Giacomo, E. Vicari, Hybrid Monte Carlo and topological modes of full QCD. Phys. Lett. B 389, 107 (1996). [arXiv:hep-lat/9607049 [hep-lat]]

45. L. Del Debbio, G.M. Manca, E. Vicari, Critical slowing down of topological modes. Phys. Lett. B 594, 315 (2004). [arXiv:hep-lat/0403001 [hep-lat]]

46. M. Luscher, S. Schaefer, Lattice QCD without topology barriers. JHEP 07, 036 (2011). [arXiv:1105.4749 [hep-lat]]

47. C. Bonati, M. D'Elia, Topological critical slowing down: variations on a toy model. Phys. Rev. E 98, 013308 (2018). [arXiv:1709.10034 [hep-lat]]